

GEOLOGIC MAP OF THE ELLENSBURG SOUTH 7.5-MINUTE QUADRANGLE, KITITAS COUNTY, WASHINGTON

by Andrew J. Sadowski, Andrew Yokel-Deliduka,
Todd R. Lau, and Anita L. Bauer

WASHINGTON
GEOLOGICAL SURVEY
Map Series 2024-05
December 2024

INTERNALLY REVIEWED



WASHINGTON STATE DEPARTMENT OF
NATURAL RESOURCES
WASHINGTON GEOLOGICAL SURVEY

GEOLOGIC MAP OF THE ELLENSBURG SOUTH 7.5-MINUTE QUADRANGLE, KITITITAS COUNTY, WASHINGTON

by Andrew J. Sadowski, Andrew Yokel-Deliduka,
Todd R. Lau, and Anita L. Bauer

WASHINGTON
GEOLOGICAL SURVEY
Map Series 2024-05
December 2024

*This geologic map was funded in part by
the USGS National Cooperative Geologic
Mapping Program, award no. G23AC00468*

*This publication has been subject to an iterative technical review
process by at least one Survey geologist who is not an author.
This publication has also been subject to an iterative
review process with Survey editors and cartographers.*



WASHINGTON STATE DEPARTMENT OF
NATURAL RESOURCES
WASHINGTON GEOLOGICAL SURVEY

DISCLAIMER

Disclaimer of Warranties. No express or implied warranty of any kind is made regarding the information contained herein, including, but not limited to, the warranty of merchantability, warranty of fitness for a particular purpose, or warranties of content, completeness, accuracy, reliability, usefulness, or that use would not infringe on privately-owned rights.

Use at Your Own Risk. The information presented here is intended for use as a general screening tool in community planning or for creating awareness and understanding of geologic information and is neither intended to constitute advice nor is it to be used as a substitute for site-specific advice from a licensed professional. You use this information at your own risk and should not act (or refrain from acting) based upon the information without independently verifying the information and, as appropriate, obtaining professional advice regarding your particular facts and circumstances.

Limitation on Liability. User agrees there shall not be liability on the State of Washington, Washington Department of Natural Resources, or their officers, agents, representatives, or employees for any damages allegedly resulting from any use of or reliance on this information. Under this limitation, there shall be no liability for any damages whatsoever, including but not limited to any damages in contract or tort for compensatory, consequential, punitive, direct, indirect, or special damages such as personal injuries, property damage, loss of profits, or any other losses or expenses.

No Endorsement. Reference herein to any specific commercial product, process, or service by trade name, trademark, manufacturer, or otherwise, does not constitute or imply its endorsement, recommendation, or favoring. Further, the views and opinions of authors expressed herein do not necessarily state or reflect those of the State of Washington or any agency thereof.

INDEMNIFICATION

Research supported by the U.S. Geological Survey, National Cooperative Geologic Mapping Program, under USGS award number G23AC00468. The views and conclusions contained in this document are those of the authors and should not be interpreted as necessarily representing the official policies, either expressed or implied, of the U.S. Government.

WASHINGTON STATE DEPARTMENT OF NATURAL RESOURCES

Hilary S. Franz—*Commissioner of Public Lands*

WASHINGTON GEOLOGICAL SURVEY

Casey R. Hanell—*State Geologist*
Jessica L. Czajkowski—*Assistant State Geologist*
Ana Shafer—*Assistant State Geologist*
Alex Steely—*Assistant State Geologist*

Washington State Department of Natural Resources Washington Geological Survey

<i>Mailing Address:</i>	<i>Street Address:</i>
1111 Washington St SE	Natural Resources Bldg, Rm 148
MS 47007	1111 Washington St SE
Olympia, WA 98504-7007	Olympia, WA 98501

Phone: 360-902-1450
Fax: 360-902-1785
Email: geology@dnr.wa.gov
Website: www.dnr.wa.gov/geology



Publications and Maps:
www.dnr.wa.gov/programs-and-services/geology/publications-and-data/publications-and-maps

Washington Geology Library Searchable Catalog:
www.dnr.wa.gov/programs-and-services/geology/washington-geology-library

Suggested Citation:
Sadowski, A. J.; Yokel-Deliduka, Andrew; Lau, T. R.; Bauer, A. L., 2024, Geologic map of the Ellensburg South 7.5-minute quadrangle, Kittitas County, Washington: Washington Geological Survey Map Series 2024-05, 1 sheet, scale 1:24,000, with 33 p. text. [https://www.dnr.wa.gov/publications/ger_ms2024-05_geol_map_ellensburg_s_24k.zip]

Cover photo: Looking north into Kittitas Valley from the entrance to Yakima River canyon. Geologist (A. Yokel-Deliduka) for scale. Photo by A. Sadowski.

© 2025 Washington Geological Survey
Published in the United States of America



ANDREW JOHN SADOWSKI

Andrew Sadowski
December 2024

Contents

Introduction	1
Geologic Overview	1
Bedrock	1
Surficial Deposits	2
Tectonic Framework	2
Methods	3
Geologic Mapping	3
Potential-Fields Geophysical Methods	4
Description of Map Units	4
Holocene to Pleistocene Nonglacial Deposits	4
Holocene? to Pleistocene Glacial Deposits.....	5
Holocene to Pliocene Nonglacial Alluvial and Colluvial Deposits	6
Quaternary Eolian Deposits	8
Tertiary Sedimentary and Volcanic Bedrock.....	9
Lithologies Depicted as Overlays	15
Mass Wasting	15
Miocene Hyaloclastite	16
Discussion	16
Inclusion of the Thorp Gravel in the Upper Ellensburg Formation.....	16
Geologic Structures in the Map Area.....	16
Mass-Wasting and Landslide Occurrence	18
Subsurface Structures Interpreted from Geophysical Anomalies	18
Recommendations for Future Research	19
Acknowledgments.....	19
Author Contributions	19
References	20
Appendix A. Gravity	25
Appendix B. Rock Physical Properties	26
Appendix C. Quantitative Geophysical Modeling of Geologic Cross Sections	27
Appendix D. Geochemistry.....	28
Appendix E. Geochronology.....	29

FIGURES

Figure 1. Map of physiographic features, place names, roads, and quadrangle boundaries	2
Figure 2. Characteristic intraflow structures and stratigraphy in lava flows.....	3
Figure 3. Annotated photo showing fold-accommodation faults in Yakima canyon	17

TABLES

Table 1. Summary of ages.....	6
Table E1. U-Pb ages	30
Table E2. Infrared-stimulated luminescence (IRSL) ages	32

MAP SHEET

Geologic Map of the Ellensburg South 7.5-minute Quadrangle, Kittitas County, Washington

Figure M1. Geophysical interpretation for the map area

Geologic Map of the Ellensburg South 7.5-minute Quadrangle, Kittitas County, Washington

by Andrew J. Sadowski¹, Andrew Yokel-Deliduka¹, Todd R. Lau¹, and Anita L. Bauer¹

¹ Washington Geological Survey
1111 Washington St SE
MS 47007
Olympia, WA 98504-7007

ABSTRACT

New geological and geophysical investigations of the Ellensburg South quadrangle refine Neogene stratigraphy and characterize geologic structures in southern Kittitas Valley. Whole-rock geochemistry (n=326) locally refines the middle Miocene chemostratigraphic framework of the Columbia River Basalt Group (CRBG). Measurements of the orientations of CRBG basalt columns reveal middle Miocene paleotopography, showing possible channelization of Grande Ronde Basalt (GRB) lava flows. Late Miocene to Pliocene (?) suprabasalt volcanoclastic strata of the Ellensburg Formation are folded in the hanging wall of a frontal thrust.

Tilted bedrock strata, active thrust faults, and fault-related folds record north-south shortening in the map area. Deformation of Quaternary sediments and recent seismicity along frontal faults indicate that contraction is ongoing. Thrusts are northward-verging and gently (<15°) southwest- to south-dipping. Northwest trending folds are tighter near the range front, and some plunge southeast. Additional structures include previously unrecognized secondary fold-accommodation faults and northerly striking oblique (?) faults, several of which may exist in Yakima canyon.

New U-Pb analysis of detrital zircons from two samples produced maximum depositional ages (MDA) of 15.36 ±0.25 Ma for a sedimentary interbed in the Wanapum Basalt and 9.54 ±0.49 Ma for an upper Ellensburg Formation conglomerate. Both ages agree with previous age analyses of these units from elsewhere around Kittitas Valley. Two luminescence ages from faulted alluvial fans suggest the faulting is ~6,000 years old or younger. A luminescence age of 3.0 ±0.4 ka from a loess mound suggests post-glacial Holocene deposition of loess.

Observed gravity and aeromagnetic data are best fit by geophysical models that include structural thickening of the GRB normal magnetostratigraphic unit N1 in the hanging wall of the low-angle Manastash thrust fault. Within this same hanging wall, misalignment between linear, north-northwest-trending geophysical anomalies and an overall northwest- to west-trending structural fabric suggests that deformation may be distributed among multiple structural blocks.

INTRODUCTION

The Ellensburg South 7.5-minute quadrangle (hereafter, the map area) is in southeast Kittitas County in central Washington State (Fig. 1). The map area covers parts of the city of Ellensburg, the mouth of Yakima River canyon, parts of Manastash Ridge, and south-central Kittitas Valley, which is located east of the Cascade Range on the western edge of the Columbia basin. Kittitas Valley is a northwest-trending, rhombic structural basin bound by faults and fault-related folds (Smith, 1903a, 1903b; Schuster, 1994).

Our 1:24,000-scale geologic mapping identifies rock units and sediment exposed at the surface, locates geologic structures such as folds and faults, and provides detailed local descriptions of rock and sediment to improve understanding of the geologic history of Washington and to provide the necessary fundamental geologic data for future studies of geologic hazards and natural resources in the map area. This work builds upon prior geologic mapping at 1:100,000 scale (Waitt, 1979; Tabor and others, 1982; Schuster, 1994), nearby 1:24,000-scale mapping (Sadowski and others, 2020, 2021, 2022, 2023), detailed surficial mapping by Kelsey and others (2017), and unpublished 1:12,000-scale geologic maps by Bentley and Powell from the early 1980s compiled by Schuster (1994).

GEOLOGIC OVERVIEW

The following *Geologic Overview* and *Methods* sections are largely similar to those in Sadowski and others (2020, 2021, 2022, 2023).

Bedrock

The map area is part of the continental Miocene Columbia River flood basalt province (Reidel and Tolan, 2013a). Locally, volcanic bedrock formations of the province consist of the Grande Ronde Basalt (GRB) and Wanapum Basalt of the Columbia River Basalt Group (CRBG). CRBG lavas erupted from dike swarms in southeast Washington, northeast Oregon, and western Idaho in the Miocene (Reidel and Tolan, 2013b; Reidel, 2015). The lavas flowed great distances until they either cooled on land or quenched in water bodies (rivers, lakes, or the Pacific Ocean) producing pillow breccia, palagonite, and hyaloclastite (Tolan and others, 1989; Reidel and others, 2013a). Roughly 95 percent of the CRBG erupted between 16.7 and 15.9 Ma (Kasbohm and Schoene, 2018; Kasbohm and others, 2023). The GRB constitutes about 72 percent of the CRBG by volume (Reidel and others, 2013a).

Figure 1. Map of physiographic features, place names, roads, and quadrangle boundaries mentioned in this report. Yellow overlay shows the extent of areas within the map area covered with thin loess deposits (typically less than 6 ft thick). Purple dotted boundary in state map below approximates the extent of the Yakima fold and thrust belt (YFTB). 'Cyn.' = canyon.



2022, 2023). Pliocene and Quaternary alluvial fan and colluvium deposits with various relative elevations, surface morphologies, and ages are present in the map area; these fans and terraces are composed of either locally sourced monomict basalt cobbles or Cascade Range-sourced polymict clasts. Sparse, Quaternary, alpine, proglacial deposits are present as distal outwash (Porter, 1976; Waitt, 1979). Deposits of Quaternary loess of the Palouse Formation are ubiquitous in Kittitas Valley and the broader Columbia basin (McDonald and Busacca, 1992).

Landslide deposits and other mass-wasting landforms are common along slopes near Manastash Ridge and within Yakima River canyon (informally, Yakima canyon). The youngest surficial units in Kittitas Valley have been modified by agriculture, irrigation, and aggregate mining.

Tectonic Framework

The map area lies within the modern backarc of the Cascadia subduction zone. During the Eocene, nonmarine sediments and arc volcanic rocks filled continental, backarc, structural basins (Tabor and others, 1982; Johnson, 1985; Eddy and others, 2016, 2017; Donaghy and others, 2021). These continental basins were later filled and capped by voluminous Neogene flood basalt lavas of the CRBG, likely related to the Yellowstone mantle plume and its interaction with the subducting Farallon plate (Camp, 2013; Camp and Wells, 2021).

Basin filling was concomitant with the onset of Miocene compression and transpression, which resulted from oblique subduction and steady, regional, clockwise rotation of the crust (Reidel and others, 1984; Wells and McCaffrey, 2013; Brocher and others, 2017). Global Positioning System (GPS) velocities reveal ongoing north–northeast-directed shortening (McCaffrey and others, 2013; Wells and others, 1998). Shortening is accommodated

Volcaniclastic and feldspathic sedimentary rocks of the Ellensburg Formation unconformably overlie and interfinger with the CRBG (Schmincke, 1964, 1967a,b; Smith, 1988a,b). The two general sources for these sedimentary rocks are (1) the ancestral Cascade Range, which supplied volcanic detritus to central Washington; and (2) ancient rivers of the inland Pacific Northwest (such as the ancestral Columbia River), which supplied feldspathic and micaceous material to the Columbia basin from distal sources in the Neogene (Schmincke, 1964, 1967a,b; Smith, 1988a,b). In the map area, we informally divide the Ellensburg Formation into lower units that are interbedded with the CRBG and contain mappable, named subunits, and upper units that overlie the youngest local CRBG unit (in other words, suprabasalt). Schmincke (1964) informally refers to ‘upper Ellensburg Formation’ as sediments above basalt of the Elephant Mountain Member (not in our map area) and where that Member is absent, he refers to sediment overlying the youngest local basalt as ‘undifferentiated Ellensburg.’ This is briefly summarized by Smith (1988a). In this context, Schmincke’s undifferentiated Ellensburg includes our upper Ellensburg.

Surficial Deposits

Within the map area, a variety of Pliocene through Holocene nonglacial deposits unconformably rest on Miocene bedrock (Porter, 1976; Waitt, 1979; Sadowski and others 2020, 2021,

by extensive, kilometer-scale, west- and northwest-striking reverse faults, thrust faults, and folds in the Yakima fold and thrust belt (YFTB) (Reidel and others, 2013b; Kelsey and others, 2017; Staisch and others, 2018a,b).

Our work encompasses part of the YFTB near Kittitas Valley and aims to characterize local fault and fold geometries. Our work also builds on prior studies of local active faults by Blakely and others (2011, 2014), Ladinsky (2012), Ladinsky and Kelsey (2012), Barnett and others (2013), Bender and others (2016), Kelsey and others (2017), and Staisch and others (2018a,b).

METHODS

Geologic Mapping

We identified lithologic units from field observations made in the summer and fall of 2023. We collected over 2,600 field data points using traditional geological field methods and digitally recorded them with Esri's ArcGIS Field Maps application. We reviewed existing 1:100,000-scale geologic mapping (Waitt, 1979; Tabor and others, 1982), three overlapping, unpublished, 1:12,000-scale field map sheets (R. Bentley and J. Powell, Central Washington University, unpub. mapping, 1980–1989), and elevation data from lidar (Washington Geological Survey, 2018, 2022). We partially adopted linework from R. Bentley and J. Powell's three unpublished maps with some modification. We referred to many geologic structures originally named by Bentley (1977). Along the Manastash range front, we also adopted the alluvial fan mapping of Kelsey and others (2017) with some modification.

We used lidar derivatives—red relief images, slope shades, hillshades, contour maps, and discrete coloring of bare earth elevation—to assess bedrock and Quaternary geology, evaluate escarpments, and observe subtle changes in topography. From lidar, we mapped mass-wasting landforms by their subtle hummocky surface morphologies. We used recent orthophotos and historical Google Earth imagery (especially May 2017) to identify linear vegetation anomalies, which we interpreted as probable faults.

We report over 500 new orientation measurements of bedding, sedimentary structures, igneous foliations, joints, and faults. We compiled 39 of these measurements from unpublished mapping by R. Bentley and J. Powell. We slightly moved a small number of these compiled orientation measurements based on field observations of the locations of outcrops. To maintain legibility at map scale, some measurements are not shown on the map sheet, but all are available in the GIS data. From structural and map data, we constructed one unbalanced southwest-northeast-oriented cross section.

We reviewed multiple datasets to inform our mapping and subsurface understanding: 84 water well logs, 3 hydrocarbon exploration records (Meridian Oil, Inc. #23-35 BN (API# 046037-00009), Shell BISSA #1-29 (API# 046037-00006), and Yakima Minerals #1-33 (API# 046037-00004)), geophysical data (gravity and aeromagnetic), geochemical analyses (major and trace elements using X-ray fluorescence), clast counts, and petrographic analyses of thin sections. For sand composition, we estimated mineral percentages from thin sections. Many of the point data locations listed above are omitted from the map for clarity or are outside the map area. The Data Supplement contains all the data collected.

Characteristic intraflow structures and stratigraphy in Columbia River Basalt Group lava flows.

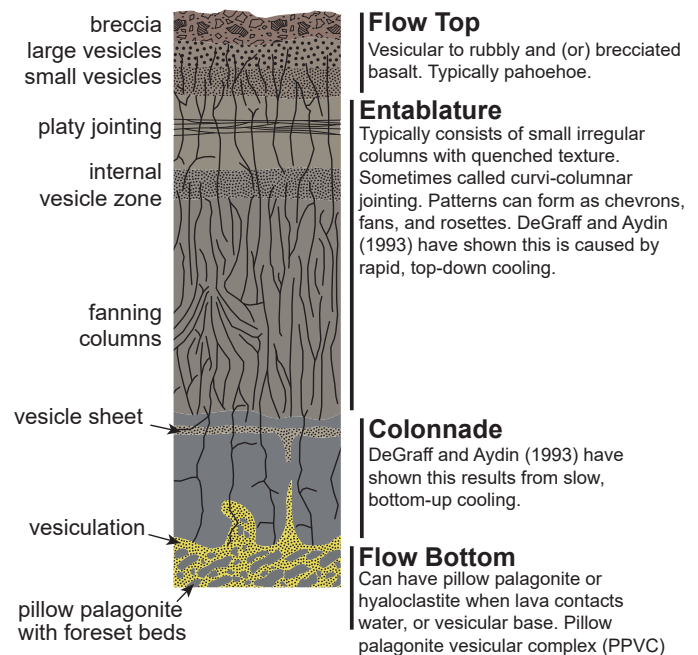


Figure 2. Characteristic intraflow structures and stratigraphy in lava flows of the Columbia River Basalt Group. Modified from Reidel and others (2013a) and Reidel (2015).

Flood basalts contain intraflow textures that help us assess flow-by-flow stratigraphy and choose geochemistry samples for comparison to previous results (see *Geochemistry*). We described flood basalt intraflow textures, which are generally found in the following order (from bottom to top, Fig. 2): hyaloclastites of pillow-palagonite breccias, basal colonnades (or boulder float of columnar jointing), entablatures (or cobble float columnar jointing), internal vesicular zones, vesicular flow tops (or cobble float), and autobreccias (Reidel, 2015).

We measured the orientation of paleo-horizontal features in CRBG rocks using two methods. We measured planar orientations of interpreted flow foliation surfaces on vesicular flow tops and columnar jointing tops. Alternatively, we measured the orientations of upright straight column sides in colonnade sections and analyzed sets of these orientations from a single column stereographically using Stereonet 10.1.0 software (Allmendinger and others, 2012; Cardozo and Allmendinger, 2013). We assume the column tops represent paleo-horizontal surfaces and are oriented perpendicular to the column sides.

However, where we observed exceptionally steep foliation in colonnade (that is, gently plunging, non-upright columns) among otherwise gently or moderately dipping foliations, we interpreted these non-upright columns as having cooled on sloped paleotopography. Such paleotopography may have channeled these lava flows such that they may be ‘intrachannel lava flows.’ Compared to ‘intracanyon lava flows’ (Reidel and Tolan, 2013b, Reidel, 2015), intrachannel lava flows may have filled paleochannels that were likely smaller in size and not as deep as paleocanyons. Based on this size disparity and a lack of hyaloclastite and sedimentary rock near the non-upright columns, we posit that the paleochannels were mostly dry and sediment poor.

Potential-Fields Geophysical Methods

We combined 243 new isostatic gravity measurements and 1,200 measurements from previous studies (Sadowski and others, 2020, 2021, 2022, 2023) to construct a refined isostatic-anomaly gravity map of Kittitas Valley (Fig. M1A). Gravity stations had 1–2 km grid spacing and an intended spacing of 250 m after being projected onto Cross Section A–A'. In addition, we applied a quantitative algorithm to identify high-amplitude, linear gradients for interpretation (referred to as 'max-spots'; Appendix A; Fig. M1A). Aeromagnetic data (Fig. M1B) are from Blakely and others (2020a,b). Modeled isostatic gravity and aeromagnetic profiles (using GM-SYS; Geosoft, Inc.) along line A–A' (Fig. M1A and M1B) quantitatively test subsurface interpretations developed from map-view data (Appendix C, Fig. M1C).

Geophysical properties were approximated using rock property measurements for density samples (27 outcrops) and magnetic susceptibility (43 outcrops) that were both collected in and outside the map area (Appendix B). We also incorporated rock property measurements from previous studies into our approximations (Sadowski and others, 2020, 2021, 2022, 2023). Appendices A, B, and C contain details of gravity, magnetic, rock property, and modeling methods. The Data Supplement contains tables with complete gravity and rock property data.

GEOCHEMISTRY

A total of 326 geochemistry samples of basaltic andesite and basalt from the map area were submitted for whole-rock geochemistry (X-ray fluorescence only) to the Peter Hooper GeoAnalytical Lab at Washington State University (WSU) (see Appendix D and Data Supplement). Most geochemistry sites are within the map area, but sites G282 and G309–326 are outside of the quadrangle, mostly to the south. Of the 326 samples published here, 23 samples were collected from the map area during previous fieldwork in 2022. These 23 sites have sample IDs with "KEK" prefixes in the Data Supplement.

Stratigraphic relationships, previous geochemical results, and geochemical variation diagrams (especially TiO₂ vs. MgO, TiO₂ vs. P₂O₅, TiO₂ vs. Zr, and Cr abundances) aided our chemostratigraphic unit classification, following previous work (for example, Martin, 1989; Reidel, 2005; Hammond, 2013; Martin and others, 2013; Reidel and Tolan, 2013a; Sadowski and others, 2020, 2021, 2022, 2023). On the map, we delineate multiple lava flows of a single chemostratigraphic unit with dark gray 'Geologic Boundary' lines. These boundary lines regularly coincide with basal contacts of lava flows at topographic slope breaks and zones above vesicular flow tops.

A machine learning (ML) model developed by Dr. Ashley Steiner (WSU) performed the initial classification of our geochemical data. However, the ML model does not consider stratigraphic context when making its classifications so its results can vary widely in confidence and stratigraphic position. As such, we relied less on the ML model and more on elemental variation diagrams and stratigraphic relationships when deciding unit classifications, especially when ML classifications had low confidence values.

GEOCHRONOLOGY

We analyzed U-Pb isotopic ratios in zircons from two sites using Laser Ablation Inductively Coupled Plasma Mass Spectrometry at the Radiogenic Isotope and Geochronology Laboratory (RIGL) at Washington State University. These results produce age spectra that we used to assess the maximum depositional age (MDA) of sedimentary deposits, or the eruptive age of pyroclastic deposits. We use the maximum likelihood age (MLA) algorithm of Vermeesch (2021) to calculate our MDA values. We also compared these results to nearby analyses from Staisch and others (2023). Table 1 summarizes the geochronology results. See Appendix E for detailed methods and see Data Supplement for analytical results.

We also analyzed Quaternary sediment from three sites using infrared-stimulated luminescence (IRSL) at the University of Illinois. Potassium feldspar was analyzed and ages are reported with 1-sigma uncertainty. These results were used to assess ages of young deposits and the age of a Quaternary surface rupture. Samples were collected under dark conditions by hammering a steel tube into a deposit and carefully removing the sediment to avoid exposing it to light (Appendix E). One site gave unambiguous results, while the other two contained anthropogenic radionuclide cesium-137, likely derived from atomic weapons testing (atmospheric fallout) or atomic weapons production during the mid-twentieth century. Fortunately, sample materials from the exposure-facing side (inner) of the sample tubes did not contain this radioactive material and we have interpretable results. See Appendix E for detailed luminescence methods.

FLUXGATE MAGNETOMETRY

We used a portable fluxgate magnetometer to assess the polarity of whole rock magnetization—reverse or normal—for members of the CRBG at 33 sites (see Data Supplement). This method is summarized in the appendix of Sadowski and others (2020). The technique is helpful for locating the change between reverse and normal magnetic remanence in the upper GRB (especially units MVgo and MVgg). See Data Supplement for analytical results.

DESCRIPTION OF MAP UNITS

Many of the unit descriptions below—particularly Quaternary units and Grande Ronde units—are similar to those from Sadowski and others (2020, 2021, 2022, 2023).

Holocene to Pleistocene Nonglacial Deposits

af Artificial fill (Holocene)—Cobbles, pebbles, sand, and boulders; poorly sorted and unconsolidated; includes foreign material at home sites, highways, railroads, trails, and recreational facilities. Unit af is at least 1.5 m thick.

ml Modified land (Holocene)—Sand-through boulder-sized material, redistributed to modify topography for industrial, agricultural, recreational, and residential uses, including, but not limited to, rock quarries and a water treatment plant. Unit ml is different from artificial fill because its composition matches the underlying

geologic unit though other original textures are no longer recognizable. Unit ml is at least 1 m thick.

Qp Peat (Holocene to Pleistocene)—Organic and organic-rich sediment; includes peat, gyttja, muck, silt, and clay; typically in closed depressions; mapped from aerial imagery in natural or man-made wetlands, bog areas, and ephemeral water bodies that align with such features; located near the Yakima River, Interstate 90, and agricultural lands. Larger natural water bodies likely contain more peat than smaller ones. The thickness and age of peat deposits is unassessed.

Qls Landslide deposits (Holocene to Pleistocene)—Clastic aggregate and scree of sand, silt, clay, cobbles, pebbles, boulders, and diamicton; medium to light yellowish brown, weathering is typically mild to moderate; generally loose and poorly consolidated; angular to subangular; unsorted, typically matrix supported; unstratified and structureless; clasts are mostly basaltic; deposits contain large quantities of silt and finer sands derived from nearby soils or sedimentary units (loess and volcanoclastic material); 5–60 m thick; unit typically found on and at the base of steep slopes. One large landslide complex in Yakima canyon is near exposures of thin, dipping sedimentary interbeds—particularly unit **Mcec**—near a monoclinial fold. These sedimentary interbeds, tilted in the monocline, may have provided favorable slide planes.

Unit Qls delineates confidently identified landslide deposits, whereas mass-wasting overlays delineate landforms with landslide-like characteristics (such as hummocky topography) but that cannot be confidently characterized as landslide deposits. Landslides and mass-wasting overlays are mapped primarily based on landforms interpreted from lidar imagery, and in both cases may be related to other processes (such as soil creep and solifluction). Absence of a mapped landslide or mass-wasting overlay does not indicate the absence of landslide hazard; site-specific investigations—and not this mapping alone—are recommended to further assess landslide hazards. We infer the age of unit Qls to be Holocene to Pleistocene.

Holocene? to Pleistocene Glacial Deposits

Deposit morphology and distinctive Cascade-sourced polymict clast composition characterize distal alpine outwash from the Cascade Range that entered the map area from the northwest through the Yakima River corridor. Glacial outwash deposits form either: (1) isolated lens-shaped terraces (unit **Qapoks**) above broad, monomict alluvial and colluvial fans, or (2) broad bands of lower-lying terraces (unit **Qaolb**) inset into older outwash terraces.

Clast compositions are diagnostically polymict in the northwestern map area including, in order of decreasing abundance, aphyric basalt, porphyritic andesite, metamorphic rocks, felsic intrusive rocks, and rare quartz and (or) chert. These compositions suggest a Cascade Range provenance with input from local Miocene and pre-Cascade arc sources.

We caution correlating alpine glaciations of central Washington with continental glaciations of western Washington in the Puget Lowland (using terms such as Vashon or pre-Vashon) on the notion that alpine and continental glaciations may be out of sync, like the timing of alpine glaciations of the Olympic Mountains and continental glaciations in the Puget Lowland (Thackray, 2001; Staley, 2015).

Qaolb Bullfrog alpine outwash of the Lakedale Drift (Holocene? to Pleistocene)—Polymict pebbly cobble gravel to pebbly sand; with gray, brown, and yellow clasts in a light to dark brown matrix; mildly weathered with weathering rinds less than 1 mm; poorly indurated, not cemented; subangular to rounded and equant to oblate clasts; with fine to coarse sand; moderately sorted; clast supported; generally structureless; deposits form broad flat to gently sloping terraces that dip to the east or southeast suggesting a westerly outwash paleo-flow direction; thickness is approximately <10 m; unit is found at elevations above the Yakima River floodplain; unit **Qaolb** is (1) at slightly lower elevations than most of alluvial fan unit **Qaf2**, (2) roughly at equal elevations with unit **Qoa**, and (3) the lowest-lying glacial outwash unit; age of Lakedale Drift is approximately correlated to the Fraser Glaciation (Porter, 1976; Waitt, 1979).

Qapoks Swauk Prairie alpine outwash of Kittitas Drift (Pleistocene)—Polymict pebbly cobble gravel to pebbly sand; clast colors include shades of gray, brown, and yellow in a light to dark brown matrix; mildly weathered, with weathering rinds on average about 1 mm thick but up to 2–3 mm thick; poorly indurated, poorly cemented; fine to coarse sand; subrounded to rounded, equant to oblate; moderately sorted, clast-supported; generally structureless; deposits form terraces with steep east-northeast-facing slopes and gentle west-southwest-facing slopes that suggest a westerly outwash source; thickness is at least 6 m; unit is found at higher elevation than unit **Qaf2**—especially near Manastash Creek in the west—and roughly at equal elevations with unit **Qaf3**. Unit **Qapoks** is slightly older than unit **Qaf2** and **Qaolb** on the basis that they are both inset into unit **Qapoks**. It is challenging to delineate unit **Qapoks** from unit **Qaf3** where exposure is poor and landforms are subdued. Diagnostically, unit **Qapoks** is polymict, whereas **Qaf3** has only basalt clasts. We identify this unit as the Swauk Prairie subdrift rather than the Indian John subdrift because to the north-northwest outside the map area the Indian John subdrift is at elevations between the Bullfrog Member and Swauk Prairie phase. Age of Kittitas Drift was inferred to be approximately 130–140 ka (Waitt, 1979). However, a recent optically stimulated luminescence analysis on fine sand inferred to be from the Swauk Prairie alpine outwash in the Ellensburg North quadrangle produced an age of 47.6 ±12.7 ka (Stephen J. Angster, U.S. Geological Survey, written commun., 2024).

Table 1. Summary of ages. Additional details are in Appendix E and the Data Supplement. 'IRSL' stands for Infrared-stimulated luminescence. 'MDA' stands for maximum depositional age. MDAs were calculated using the MLA algorithm of Vermeesch (2021) (see *Methods*).

Age site	Unit	Latitude (°N)	Longitude (°W)	Age ($\pm 2\sigma$)	Geochronological method	Age interpretation	Age source
GD01	Mcelc	46.91286	120.50566	15.36 \pm 0.25 Ma	zircon U-Pb	MDA	This study
GD02	Mvce	46.91924	120.51626	9.3 \pm 1.1 Ma	zircon U-Pb	MDA	Staisch and others (2023)
GD03	Mvce	46.92374	120.52446	10.12 \pm 0.18 Ma	zircon U-Pb	MDA	Staisch and others (2023)
GD04	Mcge	46.96291	120.60363	9.54 \pm 0.49 Ma	zircon U-Pb	MDA	This study
GD05	Mcge	46.95998	120.59866	10.16 \pm 1.4 Ma	zircon U-Pb	MDA	Staisch and others (2023)
GD06	QRcg	46.99908	120.53046	4.15 \pm 0.1 Ma	zircon U-Pb	Eruptive age	Fields (2023)
GD07	Qaf3	46.93864	120.54328	100 \pm 10 ka	Tephrochronology from Kelsey and others (2017), who determined the age by correlating sample to the Carp Lake tephra of Mount St. Helens (Carp Ash-10) (Whitlock and others, 2000).	Eruptive age	Kelsey and others (2017)
GD08	Qaf2	46.94321	120.54998	5.9 \pm 1.2 ka*	IRSL on K-feldspar.*	Burial age	This study
GD09	Qaf2	46.94476	120.55103	5.8 \pm 1.6 ka*	IRSL on K-feldspar.*	Burial age	This study
GD10	Ql	46.91791	120.56891	3 \pm 0.4 ka	IRSL on K-feldspar.	Burial age	This study

*Anthropogenic radioisotope ^{137}Cs present in sample and an anomalously young age suggest that the sample's site was modified and the IRSL age is unreliable. Expected age was 100 ka to 1 Ma.

Holocene to Pliocene Nonglacial Alluvial and Colluvial Deposits

We map the following units based primarily on their landforms (geomorphologic shapes) as expressed in lidar-based images while considering their clast compositions, clast weathering, and sedimentologic characteristics. Deposits blanket lowlands at lowest elevations (unit Qa) or form flat to gently sloping terraces with subtle topographic differences (units Qia, Qoa, QRcg). We infer the relative ages of units Qia and Qoa based on their deposits' inset relationships and proximity to active channels (unit Qa). Multiple flights of alluvial and colluvial fans are inset on the flanks of Manastash Ridge and in Yakima canyon (see units Qaf1–Qaf5).

Alluvial and colluvial deposits contain sediment ranging from boulders to clay, all in varied amounts and thicknesses. Colors range from light tannish gray to medium brown. Younger units are less cohesive and cemented than older units. In general, sand and gravel of alluvium are well rounded, moderately to well sorted, and mildly to moderately weathered. Alluvial and colluvial units are generally composed of clasts of basalt (monomict) outside of the Yakima River corridor, whereas near the Yakima River clast compositions are more diverse (polymict) and contain abundant porphyritic andesite, dacite, other volcanic rocks, some metamorphic rocks, and rare quartz. We interpret these sediments near the Yakima River as being alluvial stream channel deposits sourced mostly from the Cascade Range with contributions of basalt from nearby Miocene CRBG, distal Eocene Teanaway Formation, and (or) more distal pre-Miocene ancestral Cascade Range basalt.

Generally, we use 'local sourcing' to mean deposits containing CRBG clasts sourced from nearby CRBG exposures in Manastash Ridge. Basalt sourcing is more uncertain farther from Manastash Ridge in the northern map area, where basaltic input could come from varied sources, including the Teanaway Formation.

Qa Alluvium (Holocene)—Sand and gravel from low-est-lying stream-channel deposits on active flood plains flanking rivers and creeks; unit Qa is widely distributed throughout low elevations of the northern map area along the Yakima River and narrowly distributed in Yakima canyon and along Umtanum Creek; areas of this unit have been modified by infrastructure or agricultural cultivation. Unit Qa is inset into unit Qia. Fluvial terrace risers are more common on unit Qa surfaces, especially compared to unit Qia surfaces, and help delineate the extent of unit Qa by comparing concentrations of terrace risers. We infer the age of unit Qa to be Holocene based on ongoing alluvial deposition on portions of this unit.

Qia Intermediate-age alluvium (Holocene to Pleistocene)—Sand and gravel from expansive low-lying overbank and old channel deposits near active flood plains; poorly sorted silt to coarse sand with pebbles and cobbles. Unit Qia covers large portions of Kittitas Valley and unit Qia is inset into unit Qoa near the Yakima River; expansive Qia deposits from the north reach their southern terminus at a subtle contact between unit Qia and unit Qa in the northeast map area. Uppermost portions of unit Qia may be thinly capped by loess (unit Ql). Unit Qaf1

forms subtle fans on unit Qia surfaces suggesting unit Qia may be slightly older than alluvial fan unit Qaf1, so we infer unit Qia to be similar in age to unit Qaf2.

Qoa Older alluvium (Pleistocene)—Sand and gravel over-bank and older channel deposits that form broad, tall terraces; unit is found in the northern map area with southwest-dipping surfaces that suggest sourcing from the northeast. Unit Qoa terraces are (2–3 m) above unit Qia near Craigs Hill. West of Craigs Hill, downtown Ellensburg is located between two lobes of unit Qoa on a surface of unit Qia. Unit Qoa is inset into unit QRcg and unit Qia is inset into unit Qoa. Top surfaces of unit Qoa are about the same elevation as tops of units Qa01b and Qaf2. Unit Qoa is distinguished from other units by its inset relationships, relative elevation, sourcing direction, and monomict clast assortment. Unit Qoa may correlate with portions of the alluvial fan unit Qaf2 based on their similar elevations. The gently sloping edges of unit Qoa may grade into larger deposits of unit Qia, where the two units share a contact. The age of unit Qoa is estimated to be Pleistocene based on inset relationships and relative elevations compared to other units with known ages.

Qaf Alluvial fan and colluvial deposits (Holocene to Pliocene?)—Silt, sand, and gravel deposits; generally brown to medium gray; weathering rinds on clasts range from less than 1 to 10 mm wide and are thicker where older; loose or poorly consolidated, but contains moderately to mildly cemented zones; clay- to boulder-sized particles and generally silt to cobble gravel; angular to subrounded; moderately to very poorly sorted; generally clast supported; clasts are basalt sourced from Manastash Ridge, where CRBG exposures are common, so we infer the basalt is locally sourced CRBG. Near the Yakima River, lithologic diversity in fan deposits may be greater from intermingling of polymict river gravel and energetic basalt-rich deposits coming from Manastash Ridge. Unit thickness estimated to be less than 15 m. Sedimentological and geomorphic evidence suggests these deposits are alluvial fans transported by concentrated flows to debris flows. Colluvial deposits may be possible where deposits do not have clear fan shapes, are more poorly sorted, and have matrix support. Fans are less numerous and smaller in the map area compared to other parts of Kittitas Valley (Sadowski and others, 2020, 2023).

We subdivide this unit based on relative elevation above the modern stream level and differences in surface morphologies, and they are numbered from lowest and youngest (unit Qaf1) to highest and oldest (unit Qaf5). Older surfaces have smoother interfluves and are more deeply incised, whereas younger surfaces are inset into older surfaces and rougher but less deeply incised; weathering rinds are <1 mm thick on unit Qaf1, about 1 mm thick on units Qaf2 and Qaf3, and >1 mm thick on unit Qaf4. Fault scarps are mapped between Shushuskin and Spring Canyons on intermediate age

surfaces of units Qaf2, Qaf3, and Qaf4. Deposits of unit Qaf1 in Benwy Canyon and Yakima canyon contain an interbed of 20–50-cm-thick, very fine, white tephra (grains <<0.2 mm across—flour-like) with rare andesite fragments (<1.0 mm across). Ongoing work suggests this tephra is Mazama ash (Lydia Staisch, U.S. Geological Survey, written commun., 2024). Unit Qaf3 produced a ~470 ka age north of the map area (Sadowski and others, 2020) and a ~100 ka age from a tephra within the map area (age site GD07) (Whitlock and others, 2000; Kelsey and others, 2017). Older landforms composed of units Qaf4 and Qaf5 may be confused with unit Mcge, where exposures are poor and mapping is limited to float.

We interpret infrared-stimulated luminescence (IRSL) ages to be 5.9 ±1.2 ka (GD08) for unit Qaf3 (?) and 5.8 ±1.6 ka (GD09) for Qaf2 (Appendix E, Data Supplement).¹ These ages suggest that in this location, the Qaf3 surface containing GD08 may in fact be a faulted and uplifted Qaf2 surface. These geochronology results suggest that faulting may be ~6 ky old or younger.

Fan deposits are less abundant along the mountain front west of Yakima canyon compared to those mapped east of Yakima canyon (Kelsey and others, 2017; Sadowski and others, 2023). This may be caused by erosion of nascent alluvial fans by the Yakima River (H. Kelsey, 2024, written commun., Humboldt State University). By contrast, the ancestral Yakima River's inferred absence to the east of Yakima canyon likely allowed alluvial fans to accumulate there. However, movement on the Manastash frontal fault may have contributed to spatial patterns of alluvial fan preservation, but evidence for tectonic control on fan preservation is unclear. We map fan units with multiple ages far up Spring Canyon in the Manastash hanging wall, hinting that tectonic uplift helped preserve these fan deposits farther within Manastash Ridge.

Qg? Terrace gravel deposits (Pleistocene)—Polymict gravel in Yakima canyon; light to medium brown to yellowish brown or yellowish gray; loose, poorly cemented; pebbles, cobbles, and silt (paleosol?) with boulders and medium sand; rounded to subrounded; poorly sorted; polymict clasts may include rhyo(?)dacite; contains capping calcrete and caliche, found where exposed near a residence on the eastern map edge. Unit extent is largely based on abundant polymict float scattered atop a hill and only a single queried polygon is mapped; thickness may be up to 5 m; located on the east side of Yakima canyon in the southeast map area. Unit Qg? directly overlies and conceals CRBG units and sedimentary interbeds of the Ellensburg Formation (units McEv and McElc). These deposits are more than 50 m above the valley floor. We tentatively interpret unit Qg? as a strath terrace related to deposits from the ancestral Yakima River in agreement with nearby mapping (Kelsey and

¹Sample material from both sample tubes contained small amounts of anthropogenic cesium-137 at their atmosphere-facing (outer) end. See Data Supplement and Appendix E.

others, 2017; Sadowski and others, 2023). However, we question the existence and age of this unit because the polymict gravel may derive from polymict gravels of underlying Ellensburg Formation interbeds that are eroding in place, and a fluvial strath terrace may not be here.

QRc Sand and gravel, undivided (Pleistocene to Pliocene) (cross section only)—Pebbly cobble gravel with sand lenses; lithologies are inferred at depth in Kittitas Valley as basin fill based on unit descriptions of QRcs and QRcg. Unit may also include lithologies and polymict clast assortments akin to the Thorp Gravel. The contact between unit QRc and suprabasalt Miocene Ellensburg Formation (unit Mce) is not exposed and is difficult to identify based on well data alone given their similar lithologies. Therefore, we infer the subsurface contact may be somewhere above the combined thickness of suprabasalt Ellensburg Formation units Mvce and Mce. For more information on subsurface contacts in Kittitas Valley, please see Jones and others (2006), Jones and Vaccaro (2008), and Vaccaro and others (2009).

QRcs Volcaniclastic sandstone (Pleistocene? to Pliocene)—Variably pumiceous or pebbly sandstone; light orange to light orangish brown matrix containing light gray to white pumice fragments (which weather to a fuzzy ‘frothy’ texture), moderately weathered; moderately indurated, usually well cemented; fine- to coarse-grained sand to granules to pebbles, with rare cobbles and boulders; moderately sorted, matrix-supported; structureless to weakly laminated (planar parallel); generally angular to rounded; basalt clasts are usually angular or subangular (rarely subrounded), whereas andesite and quartz clasts may be subrounded. Sand grains are generally angular. Clast composition is a mixture of abundant locally sourced basalt clasts—among which aphyric basalt is more common than porphyritic basalt—and less common Cascade Range-sourced pumice, andesite, and hornblende dacite(?). Lithic fragments include pumice (10–20% where present, 1–8 mm across, subrounded to subangular ovals) and andesite (~1 mm diameter). Plagioclase (<0.6 mm across) and hornblende (0.6 mm long) are also common in pumice fragments and in the matrix, whereas quartz is rare. Deep red hematite(?) grains (<0.3 mm across) are present and highly birefringent minerals (clays or micas?) mat onto some voids and lithic fragment edges. Pumice and basalt content suggest mixing of distal volcaniclastic and local CRBG sources. Unit thickness is 15–30 m. The unit weathers to a diagnostic ‘pea gravel’ texture and may contain silcrete (siliceous caliche). The unit is poorly exposed as low (<0.5-m-tall) outcrops

in the southern map area on which we base our description of the unit. Unit QRcs deposits are locally capped by colluvium from nearby slopes. Based on map patterns, we infer that unit QRcs unconformably overlies Miocene bedrock, especially the Basalt of Sand Hollow (unit Mv_{wfsh}). We tentatively correlate unit QRcs with the upper portions of unit Rcg of Sadowski and others (2023) and unit QRcs of Sadowski and others (2020).

Along Cross Section A–A’ near the Manastash range front, unit QRcs may be composed of sediment derived from nearby colluvial reworking of underlying Ellensburg members (units Mvce and Mce) based on the stratigraphic position of a large unit QRcs polygon.

QRcg Oldest alluvium, gravelly unit (Pleistocene to Pliocene)—Monomict basaltic gravel; yellowish light brown to medium brown; moderately to strongly weathered with weathering rinds 1–20 mm thick; moderately compacted; cobbles and pebbles in a coarse to medium sand matrix; well rounded to rounded; moderately sorted, clast supported; sourced from CRBG and (or) Teanaway Formation; unit thickness is greater than 2 m and likely thicker at depth based on well log interpretations. The best exposure of unit QRcg is under unit Ql on the north side of Craigs Hill along the Palouse to Cascades State Park Trail on the northern map boundary.

The unit is likely sourced from Naneum Canyon and possibly from Wilson Creek to the north. The unit was previously mapped as the side stream facies of Thorp Gravel by Waitt (1979), and previously referred to as “Naneum Gravel” in field trip guides for the Kittitas Valley by Bentley (1977). Unit QRcg is younger than the Pliocene Thorp Gravel and has an MDA of ~2.33 Ma (Sadowski and others, 2020). Unit QRcg has similar lithologies and similar detrital zircon ages compared to unit Rcg of Sadowski and others (2023). On that basis, we think portions of all these units may overlap in age, are partly correlative, and wonder if unit QRcg should include unit Rcg around Kittitas Valley.

Quaternary Eolian Deposits

Ql Loess (Holocene to Pleistocene)—Eolian silt to fine sand; light to medium brown; moderately weathered; loose; angular to subangular; moderately to well sorted, matrix supported; lithology is similar to paleosols interbedded with unit Mce; structureless; varies from 2 m thick near Strande Road to 11 m thick at Craigs Hill and is otherwise thin (<1 m thick) especially across

Manastash Ridge. Thick accumulations of loess are mined near Stone Quarry Canyon near unit ml.

Loess is present nearly everywhere in the map area, but we only map it where it exceeds about 2 m thick (Fig. 1). For example, Manastash Ridge is almost completely blanketed by thin, patchy, irregularly spaced mounds of loess that are locally called Manastash mounds (Williams and Masson, 1949; Kaatz, 1959). We do not map the loess on Manastash Ridge to ensure clarity of the underlying bedrock geology. Loess in the map area is generally thicker compared to northern Kittitas Valley and loess in both areas is thinner compared to the Palouse Slope of the Columbia basin. For further information about Manastash loess see Myers (2019).

Bender and others (2016) report an IRSL age between 84.2 and 93.3 ka from loess in Yakima canyon. Four tephrochronology ages (Blanton, 1996) and two thermoluminescence ages (Lamb, 1997) of loess from the north face of Craigs Hill range from ~11–24 ka. We report a luminescence age of 3.0 ± 0.4 ka (IRSL) from a loess mound near Durr Road on Manastash Ridge (age site GD10). This new age agrees with findings of Myers (2019) that favor post-glacial loess deposition. These ages indicate unit Ql is Holocene to Pleistocene and may correlate in part with the Palouse Formation (Busacca, 1989; Sweeney and others, 2017).

Tertiary Sedimentary and Volcanic Bedrock

SEDIMENTARY ROCKS OF THE ELLENSBURG FORMATION

Like Sadowski and others (2023), we map several members of the Ellensburg Formation based on their lithologies and stratigraphic relationships with CRBG flows. Sedimentary rocks within and above CRBG flows are broadly split into lower and upper Ellensburg Formation units, respectively. The three lower units (**M_{Cec}**, **M_{Cev}**, and **M_{Celc}**) are interbedded within Wanapum and Grande Ronde Basalts and contain micaceous, tuffaceous, and basaltic sandstone to siltstone. The two upper units (**M_{Vce}** and **M_{Cge}**) overlie the uppermost CRBG locally (Wanapum Basalt) and contain volcanoclastic-pyroclastic and fluvial-conglomeratic lithologies. The lower Ellensburg Formation interbeds have names, whereas the upper ones do not and we generalize them as ‘suprabasalt Ellensburg units.’ Outside Kittitas Valley, upper Ellensburg units may correlate with named sedimentary interbeds between the Wanapum and Saddle Mountains Basalts in the Columbia basin.

Compared to the lower units, the upper Ellensburg units have greater lithologic variability, are coarser, are more strongly cemented with calcrete-silcrete, contain more volcanoclastic material, are thicker (120 m thick or more), and are less tilted. Lower Ellensburg units contain more mica (more muscovite than biotite), are variably lithified, are 35 m thick or less, and have higher abundances of pre-Cenozoic zircons compared to upper Ellensburg units.

We interpret Ellensburg Formation rocks to have fluvial, lacustrine, volcanoclastic, or colluvial origins. At depth in Kittitas

Valley, Ellensburg Formation units may form aquifers (where ash content is low) or aquitards (where ash content is high) because ash weathers to impermeable clays. In the latter case, groundwater resources may be perched in overlying lithologies.

M_{Ce} Ellensburg Formation, undivided (middle Miocene to early Pliocene?) (cross section only)—Micaceous feldsarenite, volcanoclastic sandstone, lapillistone, siltstone, and conglomerate; light to medium brown or light to medium gray; mildly to strongly weathered; mildly to moderately indurated; subrounded to sub-angular; well to moderately sorted; grain supported; composition of sand is quartz (~20–35%), feldspar (plagioclase ~10–20%, potassium feldspar ~5–15%), and lithic fragments (3–10%), with varying abundances of muscovite (0–30%). Above description is based on adjacent mapping in Kittitas Valley (Sadowski and others, 2020, 2021, 2022, 2023). At depth, unit **M_{Ce}** groups local suprabasalt Miocene sedimentary rocks (the upper Ellensburg Formation) within the cross section. Based on lithology and stratigraphic position relative to CRBG units, we locally subdivided the Ellensburg Formation into:

Upper Ellensburg Formation

M_{Cge} Conglomeratic rocks of the upper Ellensburg Formation (late Miocene to early Pliocene?)—Conglomerate with lenses of siltstone to sandstone; light to medium brown or light brownish gray with light brownish gray or pinkish tan lenses; moderately to strongly weathered; mildly to moderately cemented; pebbly cobble conglomerate with few boulders and coarse to fine sand matrix. Conglomerate is subrounded to rounded, poorly sorted, and clast supported, whereas sandy lenses have angular to subangular grains, are moderately to well sorted, and matrix supported. Conglomerate is usually structureless to uncommonly very thickly bedded (>100 cm thick) and with interbedded lenses of cross-laminated, fine pumiceous sandstone and structureless friable siltstone that we interpret as paleosol based on root casts and insect burrows. The sandstone and siltstone lenses are common in the lower portions of the unit. The conglomerate commonly contains boulder-sized rip-up clasts of siltstone. Low in the unit the conglomerate is basalt-rich with sparse (~10%) Cascade Range volcanic rocks, whereas higher in the unit the conglomerate has more diverse clast assortments with more Cascade Range volcanics, less basalt, and trace sedimentary, metamorphic, and quartzose rocks. Unit **M_{Cge}** is at least 50 m thick, but the top is poorly exposed in the map area. Unit **M_{Cge}** diagnostically contains more conglomerate and fewer volcanoclastic layers than the underlying unit **M_{Vce}**. The bottom of unit **M_{Cge}** has less pumice compared to unit **M_{Vce}** so we identify unit **M_{Cge}** where pumice is

scarce. The unit is best exposed west of Strande Road and the Manastash range front.

We interpret that (1) the conglomerate was deposited in a fluvial setting based on clast size, sorting, and clast sourcing; (2) the interbedded pumiceous sandstone was sourced from distal volcanoclastic input related to unit **MV_{CE}**; and (3) the silt of the paleosol was deposited during non-fluvial periods. From the conglomerate above the uppermost sandstone lens, we interpret an MDA of 9.54 ± 0.49 Ma (age site GD04) from U-Pb analysis of detrital zircons. Near the base of this unit by Strande Road (age site GD05) we interpret an MDA of 10.6 ± 1.4 Ma using detrital zircon analyses from Staisch and others (2023).

MV_{CE} Volcanoclastic rocks of the upper Ellensburg Formation (late Miocene)—Volcanoclastic sandstone and pumiceous pyroclastic rocks with conglomerate; greenish bluish, light to medium gray; moderately to mildly weathered; moderately indurated to friable, mildly to moderately cemented, non-welded; pumice easily dislodged; fine- to coarse-grained sandstone and pumice-rich crystal-lithic lapillistone; may contain thin (<1 cm) layers of siltstone, ash fall tuff, and accretionary lapilli tuff; sand is angular to subangular, lithic and pumice clasts subrounded; generally matrix-supported, but portions of lapillistone may be clast-supported. Very fine to fine sandstone is well sorted, medium to coarse sandstone is moderately sorted, and lapillistone is moderately to poorly sorted.

Sand includes plagioclase (~80–90%), opaque minerals (5–10%), lithic fragments (~3–10%), and hornblende (~1–5%); lithic fragments consist, in decreasing abundance, of andesite and porphyritic hornblende dacite, basalt, plutonic rock, sedimentary rock, and metamorphic rock. Approximately 70 percent of the 3–10 percent total lithic fragment fraction is andesite and hornblende dacite and likely sourced from exposures in the Cascade Range. Mica is rare and quartz is rare to absent. Pumice content (3–80%, ~1 mm to 20 cm) is diagnostic for this unit and greatest in lapillistone layers. Ash is rare to absent. Geochemical results for pumice from geochemistry site G6 (see Data Supplement) may help identify eruptive center.

The sandstone beds show planar stratification that is medium- to thick-bedded (10–100 cm) with small-scale (<1 cm) planar parallel laminations. Cross stratification is difficult to identify because exposures show a longitudinal view of troughing possibly from crossbedding. Siltstone contains plant fragment impressions. At least 11 non-welded, lenticular lapillistone layers are thin- to medium-bedded as interlayered lenses within the sandstone.

Thickness of unit **MV_{CE}** is at least ~30 m thick and may be variable given the irregular deposition of volcanoclastic deposits. Unit may grade into overlying unit **MC_{GE}**, where pumice is less abundant. Basal contact of unit **MV_{CE}** is poorly exposed, and may be

an unconformity with the Wanapum Basalt based on field relationships. Sedimentological evidence suggests a fluvial depositional setting. Unit may be correlative with regional named interbed(s) farther east (Selah, Beverly, and Mabton) as explained in unit **MV_{CE}** of Sadowski and others (2023).

We speculate that unit **MV_{CE}** is distal from Cascade Range eruptive sources based on the deposit's lack of welding and lack of vent-derived lithic fragments. The lapillistone may be a distal pyroclastic flow and (or) surge based on abundant pumice, poor to moderate sorting, and lenticular bedforms. The lapillistone is interbedded with sandstone, suggesting volcanic deposition into a fluvial setting.

Using data from Staisch and others (2023), we interpret age site GD02 as a 9.3 ± 1.1 Ma eruptive age from an airfall tephra and age site GD03 as a 10.12 ± 0.18 Ma MDA from sandstone. A U-Pb analysis of an accretionary lapilli tuff marker bed in the adjacent Kittitas quadrangle (Sadowski and others, 2023) produced an eruptive age of 8.13 ± 0.70 Ma (S. Fields, written commun., 2024, Univ. of Houston). These three ages support a late Miocene age for unit **MV_{CE}**. Unit **MV_{CE}** is best exposed along the Manastash range front and north of Stone Quarry Canyon.

Lower Ellensburg Formation

These lower units are typically micaceous to tuffaceous sandstone to siltstone, 35 m thick or less, compact, stiff, and variably lithified.

MC_{ELC} Lmuma Creek Member of the lower Ellensburg Formation (middle Miocene)—Micaceous feldsarenite; light gray to white, moderately weathered; mildly indurated or friable, mildly to moderately cemented; fine- to medium-grained sandstone; subrounded to angular; moderately to well sorted, matrix supported; structureless to poorly stratified with planar parallel laminations to thin beds and (or) subtly cross-laminated; some polymict pebble-cobble conglomerate near top; sand includes quartz (50–60%), feldspar (40–50%, plagioclase > microcline), and lithic fragments (5–10%, igneous + breccia fragments) with mica (1–5%, muscovite + biotite). Unit **MC_{ELC}** is generally less than 15 m thick, thins westward, and may thicken where mapped in synclines and structural lows. In Yakima canyon, the unit exhibits brecciation and small scale faulting (<1.5 m offset) that may be fold-related based on these features' locations within a syncline.

Unit **MC_{ELC}** is sedimentary rock above unit **MV_{WFSh}** and below unit **MV_{CE}**. Near Yakima canyon, unit **MC_{ELC}** also underlies and overlies pillow basalt of the Roza Member (unit **MV_{WR}**) and this relationship indicates that **MC_{ELC}** sediments were invaded by lavas of the Roza Member. Mapping indicates that unit **MC_{ELC}** is thin below the Roza Member and thick above it.

The contact between unit **MC_{ELC}** and overlying unit **MV_{CE}** is poorly exposed near Yakima canyon and may be unconformable. Clast compositions from units

MCelc and **MVce** are similar (see Data Supplement), but detrital zircon U-Pb age spectra are different (compare GD01 (**MCelc**) and GD03 (**MVce**)). Age site GD01 in unit **MCelc** has a 15.36 ± 0.25 Ma MDA based on the weighted mean of its two youngest zircons.

MCev **Vantage Member of the lower Ellensburg Formation (middle Miocene)**—Micaceous or volcanoclastic feldsarenite that unconformably overlies Grande Ronde Basalt unit **MVgsm** and underlies Wanapum Basalt unit **MVwfs**; light brownish gray to light gray or white-yellowish tan; moderately to strongly weathered; mildly to moderately indurated, mildly cemented; subrounded to subangular; siltstone, very fine- to coarse-grained sandstone, and pebbly cobble conglomerate; generally moderately sorted, where coarse-grained sandstone is poorly sorted and grain-supported, fine-grained sandstone is well sorted and conglomerate is moderately sorted and clast-supported. From bottom to top the unit consists of (1) 1–2 m of a basal micaceous siltstone to very fine sandstone that is structureless to thinly laminated; (2) a set of five intervals of normally graded, fine- to coarse-grained, volcanic-lithic-rich sandstone that is thickly bedded; and (3) a capping 2–3-m-thick polymict conglomerate that is structureless. These observations are similar to observations of unit **MCev** in the eastern adjacent map area (Sadowski and others, 2023).

Bimodal sand composition varies between lithic and feldspathic; coarse lithic sandstone includes plagioclase (20–30% where lithic-rich, 40–60% where lithic-poor), mica (1–7%, biotite > muscovite), some olivine? (<15%), hornblende (1–3%); compositions of lithic volcanic clasts vary between crystal-rich coarse ash (60–70% where present in west) and andesite + basalt (50–70%, or ~10% where ash is present). By contrast, in the basal, finer sandstone, lithic fragments are absent and muscovite content is very high (20–30%). Compared to unit **MCelc**, unit **MCev** generally has more mica, more lithic fragments, less quartz, and lacks microcline. Unit thickness is <20 m near Yakima canyon and thins westward. Age is approximately 16 Ma (Kasbohm and Schoene, 2018; Sadowski and others, 2023).

In the map area, lithologies, bedforms, and clast compositions suggest Vantage Member sediment accumulated in a fluvial setting with channel fill and floodplain depositional environments (Ebinghaus and others, 2014; 2020). Exposures are good in Yakima canyon, but poor elsewhere and limited to float. Mud cracks are evidence of soil desiccation possibly related to the drying of soil clays produced by weathering of ash-rich sedimentary rocks (especially volcanoclastic unit **MCev**). Unit **MCev** is common in the map area but not mapped farther north (Sadowski and others, 2020), which may suggest that southern and northern Kittitas Valley hosted different depositional settings during parts of the middle Miocene.

MCec **Coleman member of the lower Ellensburg Formation (middle Miocene)**—Micaceous feldsarenite and siltstone between the Ortley and Grouse Creek members of the GRB; medium brown to light gray; moderately weathered, weakly to moderately cemented; fine- to medium-grained; angular to subangular; well sorted, matrix-supported; structureless; sand matrix contains feldspar (40–50%), quartz (~40–50%), and varied muscovite (10–20%). Based on map patterns, the unit is less than 20 m thick and has multiple interbeds that thin out discontinuously over short distances within GRB units. Sedimentological evidence suggests a fluvial setting of channel fill and floodplain depositional environment for sediment of the Coleman member (Ebinghaus and others, 2014, 2020; Sadowski and others, 2020, 2021). Unit **MCec** is poorly exposed and only found in Yakima canyon.

Mapping of discontinuous sedimentary lenses of unit **MCec** encompassed by Grouse Creek (unit **MVgg**), Ortley (unit **MVgo**), and Winter Water (unit **MVgw**) basalts suggests that sediment of the Coleman member was likely invaded by lava flows from these three GRB units. Peperitic hyaloclastite (peperite) in Ortley basalt at geochemistry site G161 supports that lavas of the Ortley member invaded sediments of the Coleman member, but poor exposures of unit **MCec** in the other two basalt units do not have this strong evidence. Unit **MCec** is less commonly associated with GRB hyaloclastite in the map area compared to areas in northern Kittitas Valley (Sadowski and others, 2021).

We attribute an abundance of landslides downslope of unit **MCec** to the weaker material properties of the unit compared to surrounding basalt units.

The unit was informally named by Bentley (1977) near Coleman Canyon of northern Kittitas Valley and mapped by Hammond (2013) as far south as the Naches River area. Farther north, it is equivalent to the Rock Island member of Hoyt (1961), the Douglas Creek member of Ebinghaus and others (2014, 2015, 2020), and the Rock Island arkosic sand of Schmincke (1967a).

VOLCANIC ROCKS OF THE COLUMBIA RIVER BASALT GROUP (CRBG)

Flood basalts of the CRBG are documented in Special Paper volumes by Reidel and Hooper (1989) and Reidel and others (2013c). We follow their stratigraphic nomenclature and list previously used nomenclature from unpublished maps near the end of our unit descriptions. References to paleomagnetic results are summarized in Reidel (2015). We map members and sub-members of the GRB and Wanapum Basalt of the CRBG.

MVw **Wanapum Basalt, undivided (middle Miocene) (cross section only)**—Porphyritic and aphyric basalt to basaltic andesite; dark gray to grayish brown; dense; mostly microporphyritic to weakly glomerocrystic, commonly with groundmass crystals larger than 1 mm and less commonly aphyric than GRB units. Groundmass

textures are microcrystalline, equigranular, or seriate; plagioclase microlite laths are generally unoriented, but otherwise may be weakly oriented.

Compared to GRB units, Wanapum Basalt units are generally more porphyritic/glomerocrystic, thinner and less voluminous (Reidel and others, 2013a), less laterally continuous, more commonly contain hyaloclastite and platy entablature, and have common silica infilling (opal-AG, ‘amorphous-gel’) of microscopic voids. Wanapum Basalt units show weathering into yellowish brown exposures. The unit unconformably overlies the Vantage Member (unit M_{CEV}), and upper Ellensburg Formation units unconformably onlap this unit. In Yakima canyon, we estimate less than ~70 m of Wanapum Basalt, and it thins westward. The Priest Rapids Member thins completely just east of the map area. Sedimentary interbeds are common in Wanapum Basalt subunits. Unit M_{VW} includes all local Wanapum Basalt subunits at depth in the cross section. Wanapum Basalt is subdivided based on geochemistry into subunits that include:

M_{VWR} **Roza Member (middle Miocene)**—Porphyritic basalt and basaltic andesite with a medium to fine groundmass; dark gray to grayish brown, weathers dark to medium brown; dense; diagnostically porphyritic; centimeter-scale (4–14 mm) plagioclase phenocrysts (total phenocrysts: 5–10%), generally contains about a dozen phenocrysts per hand-sized sample, but top of unit M_{VWR} can be more aphyric. Several Roza compositional types exist in other areas but we found only Roza compositional unit Type IIA of Martin (1989). Unit is less than ~20 m thick. Well exposed in Yakima canyon but not exposed farther west. Based on map patterns, the unit likely pinches out completely in the central map area. Sedimentary rocks of the Lmuma Creek Member (unit M_{CEIC}) are locally found above and below unit M_{VWR} and near these contacts there is typically pillow breccia of unit M_{VWR} , which we interpret as peperitic hyaloclastite. Field relationships between the interbed and pillow breccia strongly suggest that Roza lavas invaded sediments of the Lmuma Creek Member during the Miocene (~15 Ma). Unit M_{VWR} has a $^{40}\text{Ar}/^{39}\text{Ar}$ age of 14.98 ± 0.17 Ma (Barry and others, 2013). Unit M_{VWR} has transitional magnetic polarity (Audunsson and Levi, 1997; Reidel and others, 2013a). Unpublished mapping by Bentley and Powell in the early 1980s labels this unit as “Tr.” Unit is well exposed as a thin outcrop of pillow breccia on Canyon Road.

M_{VWF} **Frenchman Springs Member, undivided (middle Miocene)**—Medium-grained basalt to basaltic andesite that is sparsely porphyritic to

weakly glomerocrystic or aphyric. This unit is typically inferred wherever geochemistry was unavailable above unit M_{CEV} and below unit M_{CEIC} , or grouped within unit M_{VW} at depth in cross section. Unit M_{VWF} (?) is usually labeled as questionable where exposures are poor and unit is inferred. With geochemistry, we identify only one Frenchman Springs sub-member in the map area: basalt of Sand Hollow (unit M_{VWFsh}). The Frenchman Springs Member is less than ~50 m thick based on map patterns, but pinches out against a fault in the northwestern map area. In general, the Frenchman Springs Member is less porphyritic than the Roza Member. The Frenchman Springs Member generally has normal remanent magnetization, but can be transitional near its base (Reidel and others, 2013a).

M_{VWFsh} **Basalt of Sand Hollow (middle Miocene)**—Medium-grained basalt and basaltic andesite that is weakly porphyritic to aphyric; medium to dark gray, weathers to dark reddish brown or reddish gray; dense; typically contains a few 1–15-mm-long euhedral plagioclase phenocrysts (usually 1–3, or <6) per hand-sized sample (total phenocrysts: ~1%), phenocrysts may cluster to form glomerocrysts; ~1-m-wide columns can internally exhibit flat to curved platy foliation; pillow breccia and palagonite (hyaloclastite) are also common. Unit is less than 50 m thick (usually ~30 m) and thins westward. Outcrops of unit M_{VWFsh} are generally widespread and near faults along the Manastash range front and south of Umtanum Creek, where we find float of sparsely porphyritic basalt. This unit directly overlies the Vantage Member (unit M_{CEV}) here because the typically intervening Gingko flow is absent, having pinched out near the Boylston Mountains farther east (Sadowski and others, 2023). Unit M_{VWFsh} directly underlies the sedimentary Lmuma Creek Member (unit M_{CEIC}). Unit M_{VWFsh} has an $^{40}\text{Ar}/^{39}\text{Ar}$ plateau age of 15.12 ± 0.38 Ma from groundmass (Barry and others, 2013). Aggregate quarries in the central map area have mined this unit.

This unit was previously called the “Kelley Hollow flow” and sometimes referred to as the “Double Barrel flow.” Unpublished mapping by Bentley and Powell

in the early 1980s labels this unit as Tfk (Frenchman Springs Kelley Hollow) or Tkh (Kelley Hollow). Note that prior usage of the name “Sand Hollow flow” (Bentley, 1977) referred to the aphyric variety of the middle Frenchman Springs Member that underlies the “Kelley Hollow flow.” “Kelley Hollow” and “Sand Hollow” units were originally split based on phenocryst content, and flow units are now grouped based on having similar geochemical compositions (Martin and others, 2013).

MVg

Grande Ronde Basalt (GRB), undivided (middle Miocene) (cross section only)—Basaltic andesite, described in detail in the following subunits and briefly summarized here. Generally, GRB rocks in hand specimen are very dark to medium gray where fresh, dark to medium brown where weathered, and dense; in thin section they show euhedral laths of plagioclase micro-lites (<1 mm in size) intermeshed in an irregular and unoriented to pilotaxitic microcrystalline groundmass texture.

GRB members are categorized into four magnetostratigraphic units (MSUs). These magnetostratigraphic units of the GRB are from oldest to youngest: ‘reverse magnetic polarity 1’ (R1), ‘normal magnetic polarity 1’ (N1), ‘reverse magnetic polarity 2’ (R2), and ‘normal magnetic polarity 2’ (N2) (Tabor and others, 1982; Reidel and Tolan, 2013; Hammond, 2013). We only observe R2 and N2 in this map area, which we divide further into chemostratigraphic subunits. Unit MVg is inferred at depth in cross section where geochemical results are unavailable (for example, portions of Grouse Creek (R2) and older GRB units are grouped at depth).

We identify several members of GRB, from old to young: Grouse Creek, Ortley, Winter Water, and Sentinel Bluffs. Each of these members contains at least one intrachannel flow based on flow foliations (*Methods*). We map a minimum of 400 m of GRB in the map area, though the base of the unit is not exposed.

MVgs **Sentinel Bluffs Member, undivided (middle Miocene) (cross section only)**—Basaltic andesite; commonly aphyric; the uppermost member of the Grande Ronde Basalt; the map area contains five subunits, from oldest to youngest: basalts of McCoy Canyon, Airway Heights, Stember Creek, Spokane Falls, and Museum. The middle three subunits are portions of the Cohasset flow, whose compositional subunits exhibit either interfingering related to sequential sheet flow inflation (Reidel, 2005) or low-temperature, secondary alteration such that interfingering is implausible (Sawlan, 2018). Cohasset subunits may locally exhibit an internal vesicular zone (IVZ) related

to flow inflation (McMillan and others, 1989; Reidel, 2015). Member has normal remanent magnetization (N2). Unit MVgs is used in the cross section to group its sub-members at depth. Where present, the IVZ may obscure the locations of vesicular flow tops due to similar appearances of other vesicular textures.

As described in *Methods*, wherever geochemical results were available, we used geochemistry and stratigraphic relationships to classify flows. Cross-comparing geochemical diagrams aids unit classification where elemental compositional fields overlap on TiO₂ vs. MgO diagrams but not necessarily on TiO₂ vs. P₂O₅ diagrams, and vice versa. Cumulatively, the Sentinel Bluffs Member is at least ~200 m thick and is common throughout the map area. The unit was previously mapped as GRB N2 MSU (Tabor and others, 1982).

Unit MVgs is used where geochemical results are unavailable and subunits are grouped at depth in the cross section. The range of chemical abundances for unit MVgs are: TiO₂: ~1.7–2.0 wt %, MgO: ~3.7–5.5 wt %, P₂O₅: ~0.28–0.69 wt %, Zr: ~149–178 ppm. With geochemistry, we subdivide the Sentinel Bluffs Member into:

MVgsm **Basalt of Museum (middle Miocene)**—Fine-grained aphyric basaltic andesite. Museum compositions are very similar to Spokane Falls compositions locally, but Zr is generally higher in Museum than in Spokane Falls. The TiO₂ vs. Zr diagram is especially useful for distinguishing compositions of Museum from those of Spokane Falls because Zr varies linearly with TiO₂, and Museum compositions reside along a trend line above the Spokane Falls trend line. From map patterns, unit thickness is >24 m in Yakima canyon to >61 m in the central map area. Unit is commonly mined for aggregate throughout Kittitas Valley. We interpret intrachannel flows of this unit based on non-upright columns in Umtanum and Yakima canyons and near the Manastash range front. The upper contact with the Vantage Member is poorly exposed. Unit contains at least two flows with colonnade, entablature, and vesicular top that are all well developed. Unit is widespread and found along Manastash Ridge and range front.

Unpublished mapping by Bentley and Powell in the early 1980s

labels this unit as Tmz (Museum), Tor (Ortley Rocky Coulee), or Trc (Rocky Coulee), but recent refinement of GRB stratigraphy (Reidel, 2005; Reidel and Tolan, 2013) lumped these compositional types together as the basalt of Museum, to which we adhere.

MVgssf Basalt of Spokane Falls (middle Miocene)—Fine-grained, aphyric basaltic andesite. Unit MVgssf has diagnostically higher Zr and lower Cr values than unit MVgssc, but unit MVgssf can be challenging to distinguish from other subunits of the Sentinel Bluffs Member that have similar geochemistry, particularly the basalt of Museum, which has even higher Zr. The TiO₂ vs. Zr diagram is especially useful for distinguishing Spokane Falls from Museum: the Zr-TiO₂ trend line for Spokane Falls lies below the Zr-TiO₂ trend line for Museum. From map patterns, unit MVgssf is ~15 m thick near Yakima canyon, ~30 m elsewhere, and more common than unit MVgssc. We interpret intrachannel flows of this unit based on non-upright columns in Umtanum and Yakima canyons. Unit MVgssf contains at least two flows and inconsistently overlies the basalt of Stember Creek (possibly near an IVZ), and—as depicted in Reidel (2005, 2015)—may interfinger with the basalt of Stember Creek. Unit MVgssf forms robust cliffs with common basal colonnade, interior entablature, vesicular flow top, and rare hyaloclastite. Unit MVgssf is common at middle elevations.

Unpublished mapping by Bentley and Powell in the early 1980s labels this unit as Toj (Ortley Jim?) or Tbt (Bingen and an unknown ‘t’ designation?).

MVgssc Basalt of Stember Creek (middle Miocene)—Fine-grained aphyric basaltic andesite. Stember Creek basalt generally has diagnostically lower Zr values compared to other subunits of the Sentinel Bluffs Member. Higher Cr and lower Zr values are particularly effective for distinguishing basalt of Stember Creek from basalt of Spokane Falls (unit MVgssf), especially where

stratigraphic relationships are unclear. From map patterns, the unit is less than ~50 m thick near Yakima and Umtanum canyons, and irregularly—or entirely—pinches out to the northwest. Unit MVgssc contains at least two flows and forms robust cliffs with common basal colonnade, interior entablature, vesicular flow top, and uncommon hyaloclastite horizons. Basalt of Stember Creek is more sparsely mapped and inconsistently interfingers with or overlies flows of Spokane Falls basalt (Reidel, 2005, 2015).

Unpublished mapping by Bentley and Powell in the early 1980s labels this unit as Toc (Ortley Cohasset?) or Tch (Chinahat/Cohasset?).

MVgsah Basalt of Airway Heights (middle Miocene)—Fine-grained basaltic andesite; medium gray; strongly weathered; dense; aphyric; exposed at two localities (geochemistry sites G66 and G170); approximate unit thickness is < 30 m, irregularly thins based on map patterns. Lacking more geochemical analyses for support, we interpret only small lenses of unit MVgsah overlying basalt of McCoy Canyon (unit MVgsmc) and underlying basalt of Spokane Falls (unit MVgssf). Given the unit’s thickness and few geochemical samples, we cannot rule out that it may be more common than we map due to under-sampling of zones between the basalts of McCoy Canyon and Spokane Falls because of lack of exposure. We report the first instance of this unit identified in the Kittitas Valley. Based on reevaluating the geochemical results of the single sample of basalt of California Creek identified in Sadowski and others (2023), it is possible that sample is instead basalt of Airway Heights.

MVgsmc Basalt of McCoy Canyon (middle Miocene)—Fine-grained aphyric basaltic andesite. From map patterns, unit MVgsmc is ~30–50 m thick. Unit MVgsmc contains at least two flows and forms robust cliffs with well-developed entablature, short basal colonnade, common vesicular flow top, and common hyaloclastite near its base. Unit MVgsmc overlies

the Winter Water Member and does not contact the Coleman member of the Ellensburg Formation (unit **MCec**). Unit **MVgsmc** is common at mid to high elevations in Yakima canyon and low elevations in Umtanum canyon.

Unpublished mapping by Bentley and Powell in the early 1980s labels this unit as **Tbb** (Bingen Bumping Hollow?) or **Tmc** (McCoy).

MVgw Winter Water Member (middle Miocene)—Fine- to medium-grained basaltic andesite; locally aphyric, but may be sparsely to abundantly glomerocrystic to porphyritic, especially farther south; medium to dark gray, weathers medium to dark brown; dense. From map patterns, unit **MVgw** is <60 m thick. We interpret intrachannel flows of this unit based on non-upright columns in Yakima canyon. Unit **MVgw** contains at least two flows and forms subdued cliffs—especially compared to overlying unit **MVgsmc**—with well-developed entablature, common stacks of segmented and tilted basal colonnade, common vesicular flow top, and hyaloclastite near its base. Unit **MVgw** underlies the Sentinel Bluffs Member (specifically, the basalt of McCoy Canyon) and overlies the Ortley member. We infer that **MVgw** floors parts of Umtanum canyon based on the constraining thickness of unit **MVgsmc**, although we lacked geochemical support for unit **MVgw** in that area. Unit **MVgw** has a normal remanent magnetization.

Note that prior usage of the name “Winter Water flow” referred to a glomerocrystic unit that overlies the aphyric “Umtanum flow” (Reidel and others, 1989), and they were divided accordingly based on phenocryst abundance. These rocks are now grouped based on their similar geochemical compositions (Reidel and Tolan, 2013), and we mostly found the aphyric variety to be abundant in the map area, especially near Yakima canyon.

MVgo Ortley member (middle Miocene)—Fine- to medium-grained aphyric basaltic andesite. Unit **MVgo** and unit **MVgg** can be difficult to distinguish because they have similar geochemical compositions, however unit **MVgo** exhibits normal remanent magnetization whereas unit **MVgg** has reversed remanent magnetization. From map patterns, unit **MVgo** is ~50 m thick. Unit **MVgo** is widespread at the lower elevations in Yakima canyon and in deep canyons along the Manastash range front. Like in northern Kittitas Valley, unit **MVgo** is exposed in a monocline. Unit **MVgo** contains two to four flows and commonly forms well-developed vesicular flow top, entablature, and palagonitic and peperitic hyaloclastite, whereas basal colonnade is rare. In Yakima canyon, the Ortley member overlies the Grouse Creek member (unit **MVgg**) and underlies the Winter Water Member (unit **MVgw**). Unit **MVgo** is part of the N2 MSU, and represents the base of N2 MSU in the map area.

Ortley basalt incorporates light gray sedimentary rock fragments of unit **MCec**. Hyaloclastite, pillow breccia, and peperite are also common in the map area, especially near Yakima canyon, and the abundance of these features strongly suggests that lavas of unit **MVgo** invaded unconsolidated, water-saturated sediment. These features and flow foliations from non-upright columns (see *Methods* for further description) suggest that invasive portions of the Ortley member were also intrachannel or intracanyon flows.

Unpublished mapping by Bentley and Powell in the early 1980s labels this unit as **Tbp** (Bingen with an unknown ‘p’ designation?) or **Tbw** (Bingen with an unknown ‘w’ designation?).

MVgg Grouse Creek member (middle Miocene)—Medium- to fine-grained aphyric basaltic andesite; groundmass crystals slightly larger than those of the Sentinel Bluffs Member. Unit **MVgg** and Ortley member (unit **MVgo**) can be difficult to distinguish because they have similar geochemical compositions, however unit **MVgg** exhibits reverse remanent magnetization whereas the Ortley member (unit **MVgo**) exhibits normal remanent magnetization. Unit represents the top of R2 MSU in the map area and its base is not observed locally. From map patterns, the unit is greater than 150 m thick and may be thicker based on mapping farther north (Sadowski and others, 2020, 2021), where the base is observed. Like northern Kittitas Valley, unit **MVgg** is exposed in a monocline. Unit **MVgg** contains multiple flows and forms robust cliffs that commonly show fanning entablatures and some places show vesicular top, platy entablature and autobreccia. Colonnade of this unit is rare. There is limited evidence for intrachannel flows. Unit **MVgg** is well exposed low in Yakima canyon.

The unit was mapped as the Howard Creek Invasive flow by Rosenmeier (1968), GRB MSU R2 by Tabor and others (1982), and the Meeks Table flow by Swanson (1976, 1978), Bentley (1977), and Hammond (2013).

LITHOLOGIES DEPICTED AS OVERLAYS

We depict overlays to highlight underlying bedrock while still showing the distribution of landforms or thin deposits.

Mass Wasting

We map mass-wasting overlays where landforms suggest mass movement on unstable slopes, but where evidence for landslide deposits is inconclusive. Overlays mark areas of hummocky or irregular surface morphology that generally lack landslide features such as head scarps, flanking scarps, and toes. We find that these mass-wasting landforms are more common at higher elevations and may indicate solifluction. In places, thin loess may overlap what appear to be mass-wasting landforms. It is unclear if such areas of overlap are mass wasting features or whether the loess produces uneven surfaces unrelated to mass wasting. The mass wasting features are common throughout the map area.

Miocene Hyaloclastite

Wherever hyaloclastite is present within or between the basaltic units of the CRBG, we delineate its extent using a map overlay. Hyaloclastite is common in Wanapum Basalt units MV_{wr} and MV_{wfs} and can also crop out near the base of units MV_{gsmc} , MV_{gssf} , and MV_{gsm} .

Where mapped, hyaloclastite consists of volcanoclastic aggregate of pillow breccia with volcanic glass (tachylyte and sideromelane) and its alteration product palagonite. Hyaloclastite is light yellowish to orangish brown, strongly weathered, compact, less dense than basaltic rocks, composed of sand- to boulder-sized clasts in a very fine-grained matrix, angular to subangular, and poorly sorted. Some exposures may contain cobble- to boulder-sized pillow breccia. Where pillows are absent, exposures are convoluted and structureless. Pillow fragments have glassy chilled margins and radial interior jointing. Hyaloclastite thickness varies but is generally less than 20 m.

In general, hyaloclastite forms where water quenches hot lava. Where lava invades saturated sediments, this generates peperitic hyaloclastite (peperite). Peperite locally contains entrained sediment among fragments of basalt and palagonite. In Yakima canyon, the invasive Ortlely basalt (unit MV_{go} , geochemistry site G161) fully encompasses white, centimeter-scale sandstone or siltstone fragments that together produce a jigsaw texture (as seen in the Coleman member). Near Canyon Road, exposures (location shown in Fig. 3) show basalt of the Roza Member (unit MV_{wr}) invaded Lmuma Creek sediment, resulting in convoluted sediment among large pillows. Peperitic hyaloclastite is strong evidence for lava having flowed into paleotopographic lows containing water and sediment.

The following mineralogical features are common near hyaloclastite and vesicular tops: fragments of petrified wood, fragments or sizeable pods (~10–30 cm diameter) of common opal, and thin patchy coatings of hyalite. Common opal (opal-AG, ‘amorphous gel’) is opaque, yellowish green to brownish yellow forming sharp glassy fragments, whereas hyalite (opal-AN, ‘amorphous network’) is clear to white, forming botryoidal silica globs that erode to smooth <4-mm-thick crusts. From the association between opaline silica mineraloids and the petrification of Miocene wood discussed by Mustoe (2023), we posit that excess silica made available by quenching lava and not involved in the petrification process precipitates as opal near hyaloclastite in CRBG rocks.

DISCUSSION

Inclusion of the Thorp Gravel in the Upper Ellensburg Formation

Although the Thorp Gravel does not crop out in the map area, lithologic similarities abound between the Thorp Gravel and conglomeratic facies of the upper Ellensburg Formation. At Craigs Hill, a tephra within a reworked lahar produced a U-Pb eruptive age of 4.15 ± 0.10 Ma (GD06; Fields, 2023). Although this Pliocene age is within the potential age range of the Thorp Gravel (4.7–3.7 Ma) (Smith 1988a,b; Smith, 1989), the volcanoclastic and conglomeratic lithologies at Craigs Hill are identical to upper Ellensburg units. Therefore, we advocate that this age and the

Thorp Gravel be grouped within the Ellensburg Formation. Doing so also implies that the unconformity between the Thorp Gravel and Ellensburg Formation is a minor intraformational unconformity and represents less than ~1.5 my of nondeposition locally using the tephra’s ~4.15 Ma age and an MDA of ~5.22 Ma from age site GD11 of Sadowski and others (2023). With prior work (Schmincke, 1967b) and recent geochronology (Fields, 2023; Sadowski and others, 2020, 2023), we suggest that the upper part of unit M_{cge} may be Pliocene and includes the Thorp Gravel.

Geologic Structures in the Map Area

Northwest- through west-trending basin-bounding folds are common along Manastash Ridge, which is part of the Yakima fold and thrust belt (YFTB). These folds consist of high-amplitude anticlines in the hanging walls of large-offset thrust faults. Thrusts and anticlines are the primary, first-order geologic structures in the map area. Mapping these structures’ geometries is the first step to assessing their activity and what hazard they may pose.

We map long, continuous, low-angle (dipping <15° SW) frontal thrust faults and higher-angle (dipping >~50° SW) reverse faults near the Manastash range front that diagonally span the map width. At least one thrust fault produces scarps in Quaternary alluvial fan unit Q_{af2} between geochemistry sites G39 and G46. Reverse faults only offset Miocene units and their Quaternary activity is unclear.

A recent, temporary deployment of three broadband seismometers on and near the Manastash range front (seismometer sites S01–03) and near an existing PNSN station (ELL) recorded <M2.0 earthquakes likely associated with the concealed portions of the Manastash frontal thrust (W. Szeliga, CWU, written commun., 2024). The observed fault scarps and seismicity may suggest the presence of Quaternary-active faults along the Manastash range front.

In the Manastash thrust hanging wall, we map a large-amplitude, northwest-trending, gently east-plunging (1–3°), northeast-verging, asymmetric anticline with a gentle (dipping <15° SW) southern backlimb and steeper (dipping 25–40° NE) northern forelimb. We also map a northwest-trending, closely spaced anticline-syncline fold pair, where the syncline (interlimb angle ~40°) may only show one limb (half-syncline) because the other limb is in the footwall of an adjacent fault. We interpret that folding is fault-related and associated with fault-propagation given the large fold’s shape and proximity to the active frontal thrust fault.

The change in the strike—and vergence—of the frontal thrust fault near Manastash Creek may be due to changes in the thrust’s geometry at depth to the west. Geometry changes may include a warping, bending, or tearing of the thrust fault’s ramp-like surface. Warping or bending could be caused by changes in slip amount along the fault plane or the interplay between brittle-ductile deformation in the CRBG strata (amounts of slip versus intensity of folding), whereas tearing may be attributed to cross faulting oblique to thrust strike.

In the southwestern map area, a gently east-plunging anticline is subparallel to the conspicuously straight trace of Umtanum Creek. The creek follows the anticline hinge and structural control may explain its straightness where water favors flowing through joints and fractures along the fold hinge.

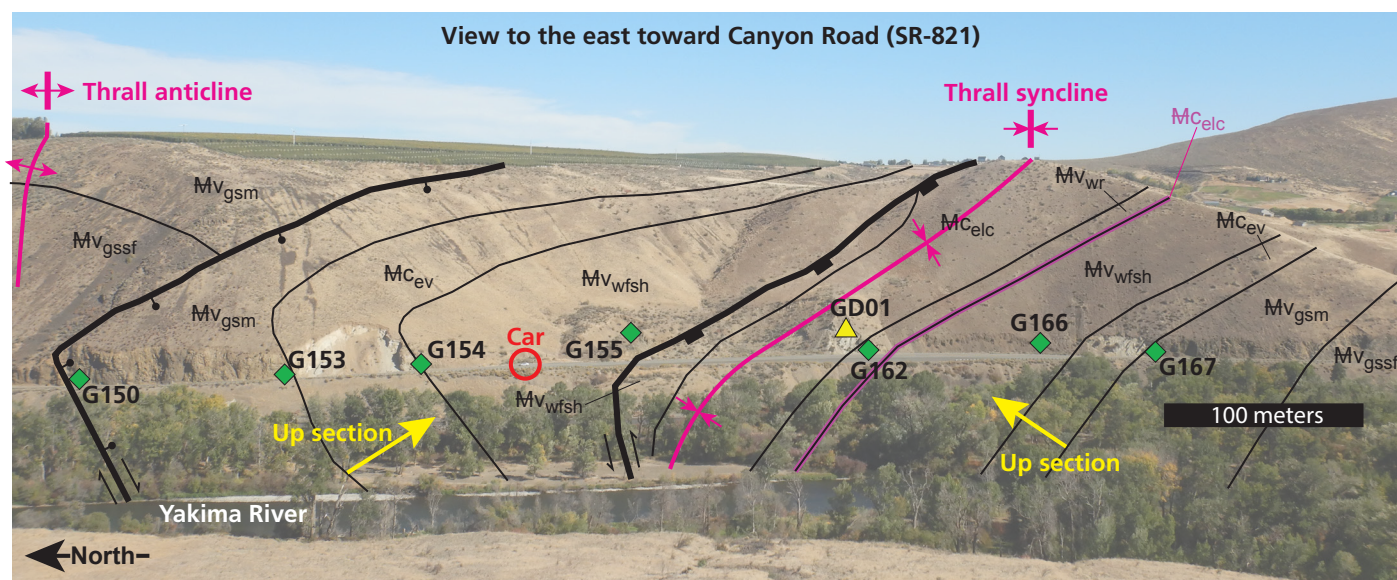


Figure 3. Annotated photo showing fold-accommodation faults (thick black lines) in Yakima canyon near age site GD01 (Table 1), including an 'out-of-syncline-type' reverse fault and a 'limb-wedge thrust-type' normal fault with layer-parallel slip. Additional intra-unit fault surfaces are near geochemistry sites G154, G155, G162 (invasive Roza pillows), and G167. Yellow arrows point up section from the base of the Vantage Member (M_{cev}) within the Thrall syncline. Unit labels and descriptions can be found in *Description of Map Units*. Manastash anticline is farther south (right) and not pictured. Green diamonds are geochemical samples.

FOLD-ACCOMMODATION FAULTS NEAR YAKIMA CANYON

Orientations of several fault surfaces show slickenlines indicating oblique-slip motion along faults that strike parallel to and within a northwest-trending syncline that spans Yakima canyon.

Near the fold hinge, fault surfaces along a single fault trace are high angle (dipping 69–80°S) and subparallel (or oblique) to tilted strata (Fig. 3). We can trace the fault across Yakima canyon but not across the entire map width. We infer decimeter to hectometer displacement based on map patterns and an inferred sense of slip. Sense of slip on this fault is difficult to determine from map patterns alone. However, ongoing regional compression since the Miocene suggests that this fault may be favorably oriented for oblique-reverse slip. Additionally, the concave zone of syncline hinges can contract to produce reverse faults during contraction. Therefore, we interpret this fault near the fold axis to be a reverse fault, specifically an 'out-of-syncline' thrust fault (Mitra, 2002) based on its matching shape, sense of slip, orientation and location relative to the fold hinge. Note, out-of-syncline faults may be synonymous with bending-moment faults (for example, Li and others, 2018).

Away from the fold hinge, fault surfaces from both limbs have orientations parallel (or subparallel) to steeply tilted strata, which suggests that these faults exhibit high-angle, layer-parallel, oblique-normal, or oblique-reverse senses of slip. We infer meter to decimeter throw based on map patterns. We cannot trace these faults across Yakima canyon, so we infer that they are not continuous over large distances. Fault geometries in the syncline limbs may match those of either 'limb wedge thrust' faults (Mitra, 2002) or flexural-slip faults (see Li and others, 2017) based on their layer-parallel slip, how their fault planes are similarly oriented to surrounding strata, and their locations on the fold.

Both out-of-syncline and limb wedge thrust faults (along with bending-moment and flexural-slip faults) are types of

fold-accommodation faults, and our mapped fault geometries match those of fold-accommodation faults. These fold-accommodation faults accompany fold development in the YFTB and are secondary to development of the major fold-bounding thrust faults (first-order structures). Fold-accommodation faults were previously unrecognized in Kittitas Valley. Recognizing fold-accommodation faults is key to interpreting the structural geology of the map area and the fold-belt province at large.

NORTHERLY STRIKING FAULTS (NSFs)

Northerly striking, high-angle cross faults (or transverse faults) are obliquely oriented relative to first-order, fold-bounding thrust faults regionally within the prominent folds of the YFTB. Many of these cross faults are oblique-slip to strike-slip and can be transfer faults among the major thrust faults (for example, the Warwick fault zone in Woodring, 2020; O'Connor and others, 2021). In the map area and around Kittitas Valley (Sadowski and others, 2021, 2022, 2023) we identify northerly striking faults (NSFs) that may share characteristics with these regional cross faults.

We map numerous, short, discontinuous to weakly anastomosing NSFs that strike northwest through northeast primarily based on geologic evidence in Yakima canyon and subtle topographic and vegetation lineaments in Google Earth satellite imagery (May 2017) elsewhere. Strike-slip offset of active or abandoned stream channels was not observed.

The following geologic features suggest an NSF in Yakima canyon: (1) abundant fault breccia, numerous north- and east-striking joints and fault surfaces near a topographic saddle (near geochemistry site G178), (2) an apparent ~660 m right-step of the west-trending Manastash anticline across the canyon, and (3) several flow foliations that anomalously dip toward this NSF, which suggests faulting perturbed these nearby orientations. Also, an NSF may best explain the disconnection between the

upper contact of unit Mv_{gg} (near geochemistry site G176) across Yakima canyon to the adjacent map area to the east. Lastly, we speculate that the zone of weakness formed by this NSF in Yakima canyon may have caused the Yakima River to exit at this location.

Outside of Yakima canyon, lineaments lack fault exposures, and map patterns show only meter-scale vertical offset, if any. Given these small vertical offsets, we suspect NSFs may exhibit some strike-slip motion because NSFs are also favorably oriented for strike-slip motion in the current stress regime. On this basis, if NSFs are strike-slip to oblique-slip faults, then it is possible they are transfer faults like cross faults elsewhere in the YFTB, and the generative mechanism for NSFs can be explained similarly (Tavani and others, 2015). Like other secondary structures in the map area, understanding NSFs is critical to interpreting the YFTB's deformation history and how second- and first-order structures may accommodate slip. Alternatively, NSFs may form in relation to changes in the underlying geometry of the thrust fault surface or may be discontinuous surface manifestations of deeper throughgoing crustal structures that subdivide the map area into different structural blocks (see *Subsurface Structures Interpreted from Geophysical Anomalies*).

Mass-Wasting and Landslide Occurrence

Mass-wasting landforms and landslide deposits form on unstable slopes in the map area, and their occurrences may in some cases be associated with geologic conditions underlying steep slopes. Some landslides and many mass-wasting overlay polygons align with the trends of fault-related folds that tilt bedrock. West of Yakima River, we map a large landslide complex where weak layers of sedimentary Coleman member have been steeply tilted by folding and faulting. The bedrock strata flanking this landslide are folded and near at least one fault.

Smaller landslides and mass-wasting features (formed by soil creep or freeze-thaw) are mapped on hummocky slopes containing sedimentary rocks of the Vantage Member or loess and loess-rich soils. Sedimentary deposits in the map area are weaker and less competent than the surrounding volcanic strata, which exhibit greater rock strength.

Based on the above observations, slopes susceptible to mass-wasting may be associated with a combination of stratigraphic and structural geologic conditions. These conditions may include the presence of weak rocks and structurally deformed strata. Site-specific investigations are strongly recommended when evaluating unstable slopes.

Subsurface Structures Interpreted from Geophysical Anomalies

We present an isostatic gravity map (Fig. M1A), aeromagnetic anomaly map (Fig. M1B), and geophysical model (Fig. M1C) to inform our interpretations of the geologic cross section and geologic map.

MANASTASH THRUST FAULT

Steep, linear gradients and short-wavelength and high-amplitude anomalies are prominent features in both the gravity and magnetic anomaly maps (LGG, Fig. M1A; SWH and SWL, Fig. M1B;

LGG—Large Gravity Gradient; SWH—Short-Wavelength High; SWL—Short-Wavelength Low) in the central portion of the study area.

We model the Manastash frontal fault as a low-angle thrust fault (MTF—Manastash thrust fault, Fig. M1C), which explains all three of these geophysical features (LGG, Fig. M1A; SWH and SWL, Fig. M1B) and agrees with previous modeling (Sadowski and others, 2023; Staisch and others, 2018). In our study area, both gravity and magnetic gradients at the northeast end of the MTF tightly constrain the southwestward dip of the thrust, and the northeastward dip in a footwall fold at 5 mi distance along the model section A–A'. The main contributor to the large aeromagnetic anomalies (SWL and SWH respectively, Fig. M1B) is the R2 and N2 contact in the footwall. Within the footwall, a syncline generates abundant accommodation space for post-CRBG sediments, which contribute to the northward decrease in gravity across LGG (Fig. M1A and Fig. M1C). A shallow dip for the Manastash thrust fault (MTF in Fig. M1C) is supported by the need for relatively dense rocks that we model as Winter Water Member ($\rho = 2,800 \text{ kg/m}^3$) near the surface to match the gravity high (SB1, structural block 1, Figs. M1A and M1C).

The aeromagnetic anomalies (SWH and SWL, Fig. M1B) trend northwest at acute angles to the gravity gradient (LGG, Fig. M1A), which trends west-northwest. This misalignment suggests that the fold axis of the footwall syncline is not parallel to the strike of the thrust fault.

N1/R2 CONTACT

A broad magnetic high (BMH, Figs. M1B and M1C) represents the second-highest-amplitude aeromagnetic anomaly within our study area. Our modeling of this anomaly indicates large amounts of normally magnetized material within the shallow (<1,000 m) subsurface. We hypothesize that uplifted and structurally thickened N1 (UN1—Uplifted N1, and UN1a—Uplifted N1 subblock, Fig. M1C) explains the observed potential field data.

In the center of the map area, near-horizontal and undeformed basalt of Museum is exposed in Manastash Ridge (unit Mv_{gsm} a member within N2 in Fig. M1C). This observation prohibits N2 deformation as the cause of the 'BMH' anomaly because it would be difficult to translocate the necessary amount of N2 material deep enough without deforming the Museum member. Rather, our modeling suggests that the thickness changes in R2 units within the hanging wall are due to uplift of the N1 units prior to the deposition of the R2 units, and not due to deformation after the deposition of R2.

We acknowledge our model produces a poor fit to the aeromagnetic data near 'RMH' and 'UN1a' (Fig. M1C) because of uncertainties introduced by the relatively large distance between model data points and the profile line. Here, we suspect unresolved structures could be related to the complex structural block intersection or above uncertainties.

STRUCTURAL BLOCKS 1 AND 2

We interpret observed linear relative magnetic highs (RMH, Fig. M1B) as evidence of an approximately model-parallel, west-side-up, high-angle reverse fault that crosses the geophysical model line several times (HF, high-angle fault, Fig. M1C) caused uplift of 'UN1' and 'UN1a'. The structure is discontinuous in

our model due to off-profile points being projected to the profile plane. Therefore, we suggest the presence of at least two different structural blocks (SBs) (SB1 and SB2, Figs. M1A, M1B, and M1C) within the hanging wall of the Manastash thrust fault. The boundaries of these blocks are marked by strong aeromagnetic lineaments (such as ML—Magnetic Lineament, Fig. M1B). The block boundaries are also associated with topographic lineaments and, in some cases, are associated with changes in the trend of gravity gradients (NE—Northeast Trending Gradient, Fig. M1A). The presence of these structural blocks is supported by our modeling, though the exact boundaries of the SB1 and SB2 remain unclear and could include the smaller blocks outlined in thin white lines (X and Y, Figs. M1A and M1B). Boundaries of higher confidence are supported by multiple types of geophysical and topographic data, while less clear boundaries are only supported by aeromagnetic lineaments and knowledge of existing structures outside the study area and (or) model.

Structural block SB1 is defined on the east and west by linear low aeromagnetic anomalies (ML, Figs. M1A and M1B) and to the north and south by the Manastash and Umtanum thrust faults (respectively, MTF and UTF, Figs. M1A, M1B, and M1C). The gravity anomaly within SB1 is lower relative to that of SB2 (Fig. M1A) with gravity contours roughly parallel to all sides of SB1.

Structural block SB2 is defined by broad and high magnetic and gravity anomalies (Fig. M1A and M1B), which we interpret as uplifted N2 units. SB2 is bounded on its northern side by the Manastash thrust fault and on its southern side by the Manastash and Umtanum thrust faults. The gravity gradient between SB1 and SB2 (NE, Fig. M1A) trends northeast-southwest and helps define the SB1-SB2 boundary. A high-angle reverse fault (HF, Fig. M1C), within the Manastash hanging wall, accommodates uplift of the N2 unit within SB2.

RECOMMENDATIONS FOR FUTURE RESEARCH

- Refine the timing of fluvial deposition of unit QRCS by using U-Pb geochronology of detrital zircons and (or) tephrochronology of the sub-centimeter pumice fragments. This research will help correlate Quaternary and Pliocene surficial units across Kittitas Valley.
- At present, the youngest basalt in the subsurface is inferred to be Saddle Mountains Basalt with an unclear basis (Kelsey and others, 2017), or Wanapum Basalt (Priest Rapids Member or older?) based on mapping (Sadowski and others, 2023). Determining the CRBG formation that forms the top-of-basalt at depth near the range front using detailed downhole geochemical logging will better constrain structural and geophysical models.
- Elucidate the detailed interflow relationships and eruption chronology among “Cohasset-flow” compositional types, especially the Stember Creek and Spokane Falls subunits, from cliff outcrops north and south of Umtanum Creek using detailed sketches, photography (telephoto or drone), and closely spaced geochemical samples. This work may further the debate between Sawlan (2018) and Reidel (2005).

- Deploy a small aperture seismic array to record, locate, and characterize the hypocenters and focal mechanisms of small magnitude seismicity near the Manastash range front.
- Perform paleoseismic investigations on faults near the Manastash range front to elucidate Quaternary fault activity and potential hazards.
- Investigate the paleoclimate and paleoenvironment during loess deposition using pollen analysis (palynology) from Manastash mounds to better assess the timing of loess deposition following work from Myers (2019).

ACKNOWLEDGMENTS

We thank, from CWU: Walter Szeliga, Lisa Ely, Bre MacInnes, Carey Gaiz, Nick Zentner, and faculty of the Geology Department for meaningful conversations and field trips. From WGS, we thank: Alex Steely, Michael Polenz, and Trevor Contreras for initial reviews of the map, cross section, and report text. We also thank Ashley Cabibbo for GIS data stewardship and quality control. From USGS, we thank Lydia Staisch and Steve Angster for help synthesizing past and ongoing regional work. Of Humboldt State University, we thank Harvey Kelsey for helpful correspondence regarding the Manastash range front. Of emeritus investigators, we thank Jack Powell for sharing his work, clarifying geologic questions, and introducing us to helpful landowners. Of WSU, thanks to Ashley Steiner, John Wolff, and the whole staff at the WSU Peter Hooper GeoAnalytical lab in Pullman, WA for geochemical analyses and CRBG unit classification using their Machine Learning (ML) model, especially under unforeseen technical difficulties. We also thank Thomas Lapen and Shawn Fields of University of Houston for sharing their new age data from Kittitas Valley. We also thank Skye Cooley for meaningful discussions about Columbia basin stratigraphy. Of private citizens, we thank the Acheson Family, Lyons Family, Thayer Family, Broadlick Family, Møllergaard Family, Bart Bland, Arlan Kummer, Bender Family, and countless other private landowners, ranchers, farmers, and businesses for general assistance or land access. We also thank Zirkle Fruit, Kittitas Reclamation District (KRD), and Cascade Irrigation District for access through or around their properties. Lastly, we thank the numerous rattlesnakes in and around Umtanum canyon for keeping our awareness keen.

AUTHOR CONTRIBUTIONS

Geologic mapping was performed by A. Sadowski and A. Yokel-Deliduka together in most of the map area. A. Yokel-Deliduka performed solo fieldwork in portions of Umtanum canyon, Yakima canyon, and between Shushuskin and Stone Quarry canyons. Geophysical data were collected by A. Bauer and T. Lau, reduced by A. Bauer, and interpreted and modeled by T. Lau with contributions from M. Anderson and A. Bauer. Writing of the pamphlet was completed by A. Sadowski, A. Yokel-Deliduka, and T. Lau. A. Sadowski interpreted the geochemical and geochronological results and performed the petrography. A. Sadowski wrote most of the text with T. Lau providing contributions in Methods, Appendices A, B, C, and Discussion of

Geophysical Anomalies including geophysical figures. A. Yokel-Deliduka provided contributions to the Introduction, Geologic Overview, Methods, Data Supplement, reviews of preliminary geochemical interpretations, and Google Earth reconnaissance. GeMS data schema and Data Supplement were populated by A. Sadowski. Map GIS linework, geologic analysis, and geologic cross section construction were performed by A. Sadowski and A. Yokel-Deliduka.

REFERENCES

- Allmendinger, R. W.; Cardozo, Nestor; Fisher, D. M., 2012, Structural geology algorithms: Vectors and tensors: Cambridge University Press, 289 p. [https://doi.org/10.1017/CBO9780511920202]
- Audunsson, Haraldur; Levi, Shaul, 1997, Geomagnetic fluctuations during a polarity transition: *Journal of Geophysical Research*, v. 102, p. 20,259–20,268. [https://dx.doi.org/10.1029/96JB02534]
- Barnes, D. F.; Oliver, H. W.; Robbins, S. L., 1969, Standardization of gravimeter calibrations in the geological survey: *Eos, Transactions American Geophysical Union*, v. 50, no. 10, p. 626–627. [https://doi.org/10.1029/EO050i010p00526]
- Barnett, E. A.; Sherrod, B. L.; Norris, Robert; Gibbons, Douglas, 2013, Paleoseismology of a newly discovered scarp in the Yakima fold-and-thrust belt, Kittitas County, Washington: U.S. Geological Survey Scientific Investigations Map 3212. [http://pubs.usgs.gov/sim/3212]
- Barry, T. L.; Kelley, S. P.; Reidel, S. P.; Camp, V. E.; Self, Stephen; Jarboe, N. A.; Duncan, R. A.; Renne, P. R., 2013, Eruption chronology of the Columbia River Basalt Group. *In* Reidel, S. P.; Camp, V. E.; Ross, M. E.; Wolff, J. A.; Martin, B. S.; Tolan, T. L.; Wells, R. E., editors, The Columbia River flood basalt province: Geological Society of America Special Paper 497, p. 45–66. [https://doi.org/10.1130/2013.2497(02)]
- Bender, A. M.; Amos, C. B.; Bierman, Paul; Rood, D. H.; Staisch, Lydia; Kelsey, Harvey; Sherrod, Brian, 2016, Differential uplift and incision of the Yakima River terraces, central Washington State: *Journal of Geophysical Research Solid Earth*, v. 121, no. 1, p. 365–384. [https://doi.org/10.1002/2015JB012303]
- Bentley, R. D., 1977, Stratigraphy of the Yakima basalts and structural evolution of the Yakima ridges in the western Columbia Plateau. *In* Brown, E. H.; Ellis, R. C., editors, *Geology excursions in the Pacific Northwest*: Geological Society of America, p. 339–390.
- Black, L. P.; Kamo, S. L.; Allen, C. M.; Davis, D. W.; Aleinikoff, J. N.; Valley, J. W.; Mundil, Roland; Campbell, I. H.; Korsch, R. J.; Williams, I. S.; Foudoulis, Chris, 2004, Improved $^{206}\text{Pb}/^{238}\text{U}$ microprobe geochronology by the monitoring of a trace-element-related matrix effect; SHRIMP, ID-TIMS, ELA-ICP-MS and oxygen isotope documentation for a series of zircon standards: *Chemical Geology*, v. 205, no. 1–2, p. 115–140. [https://doi.org/10.1016/j.chemgeo.2004.01.003]
- Blanton, William, 1996, Main stream gravel deposits, terraces and associated tephros of the lower Yakima River canyon, Kittitas County, Washington: Central Washington University Undergraduate Thesis.
- Blakely, R. J.; Sherrod, B. L.; Weaver, C. S.; Wells, R. E.; Rohay, A. C.; Barnett, E. A.; Knepprath, N. E., 2011, Connecting the Yakima fold and thrust belt to active faults in the Puget Lowland, Washington: *Journal of Geophysical Research Solid Earth*, v. 116, no. B7. [https://doi.org/10.1029/2010JB008091]
- Blakely, R. J.; Sherrod, B. L.; Weaver, C. S.; Wells, R. E.; Rohay, A. C., 2014, The Wallula fault and tectonic framework of south-central Washington State, as interpreted from magnetic and gravity anomalies: *Tectonophysics*, v. 624–625, p. 32–45. [https://doi.org/10.1016/j.tecto.2013.11.006]
- Blakely, R. J.; Sherrod, B. L.; Weaver, C. S., 2020a, High-resolution aeromagnetic survey of the Wenatchee area, Washington: U.S. Geological Survey data release. [https://doi.org/10.5066/P9EURKIG]
- Blakely, R. J.; Sherrod, B. L.; Weaver, C. S., 2020b, High-resolution aeromagnetic survey of the Cle Elum area, Washington: U.S. Geological Survey data release. [https://doi.org/10.5066/P9C9MADW]
- Brocher, T. M.; Wells, R. E.; Lamb, A. P.; Weaver, C. S., 2017, Evidence for distributed clockwise rotation of the crust in the northwestern United States from fault geometries and focal mechanisms: *Tectonics*, v. 36, no. 5, p. 787–818. [https://doi.org/10.1002/2016TC004223]
- Busacca, A. J., 1989, Long Quaternary record in eastern Washington, U.S.A., interpreted from multiple buried paleosols in loess: *Geoderma*, v. 45, no. 2, p. 105–122. [https://doi.org/10.1016/0016-7061(89)90045-1]
- Camp, V. E.; Wells, R. E., 2021, The case for a long-lived and robust Yellowstone hotspot: *Geological Society of America Today*, v. 31, no. 1, 10 p. [https://doi.org/10.1130/gsatg477a.1]
- Camp, V. E.; Reidel, S. P.; Ross, M. E.; Wolff, J. A.; Martin, B. S.; Tolan, T. L.; Wells, R. E., 2013, Origin of Columbia River basalt: Passive rise of shallow mantle, or active upwelling of a deep-mantle plume: *Geological Society of America Special Paper 497*, p. 181–199. [https://doi.org/10.1130/2013.2497(07)]
- Cardozo, Nestor; Allmendinger, R. W., 2013, Spherical projections with OSXStereonet: *Computers & Geosciences*, v. 51, p. 193–205. [https://doi.org/10.1016/j.cageo.2012.07.021]
- Chang, Zhaoshan; Vervoort, J. D.; McClelland, W. C.; Knaack, Charles, 2006, U-Pb dating of zircon by LA-ICP-MS: *Geochemistry, Geophysics, Geosystems*, v. 7, no. 5 [https://doi.org/10.1029/2005GC001100]
- DeGraff, J. M.; Aydin, Atilla, 1993, Effect of thermal regime on growth increment and spacing of contraction joints in basaltic lava: *Journal of Geophysical Research, Solid Earth*, v. 98, no. B4, p. 6,411–6,430. [https://doi.org/10.1029/92JB01709]
- Donaghy, E. E.; Umhoefer, P. J.; Eddy, M. P.; Miller, R. B.; LaCasse, Taylor, 2021, Stratigraphy, age, and provenance of the Eocene Chumstick basin, Washington Cascades; Implications for paleogeography, regional tectonics, and development of strike-slip basins: *Geological Society of America Bulletin*, v. 133, no. 11–12, p. 2,418–2,438. [https://doi.org/10.1130/B35738.1]
- Ebinghaus, Alena; Hartley, A. J.; Jolley, D. W.; Hole, Malcolm; Millett, John, 2014, Lava-sediment interaction and drainage-system development in a large igneous province: Columbia River flood basalt province, Washington State, U.S.A.: *Journal of Sedimentary Research*, v. 84, no. 11, p. 1041–1063. [https://doi.org/10.2110/jsr.2014.85]
- Ebinghaus, Alena; Jolley, D. W.; Hartley, A. J., 2015, Extrinsic forcing of plant ecosystems in a large igneous province: The Columbia River flood basalt province, Washington State, USA: *Geology*, v. 43, no. 12, p. 1,107–1,110. [https://doi.org/10.1130/G37276.1]
- Ebinghaus, Alena; Taylor, Ross; Barker, Aaron; Hartley, A. J.; Jolley, D. W.; Hole, M. J., Development of inter-lava drainage systems in LIPs: The Columbia River flood basalt province (U.S.A.) as a case study: *Journal of Sedimentary Research*, v. 90, no. 10, p. 1346–1369. [https://doi.org/10.2110/jsr.2020.64]
- Eddy, M. P.; Bowring, S. A.; Umhoefer, P. J.; Miller, R. B.; McLean, N. M.; Donaghy, E. E., 2016, High-resolution temporal and stratigraphic record of Siletzia's accretion and triple junction migration from nonmarine sedimentary basins in central and western Washington: *Geological Society of America Bulletin*, v. 128, no. 3–4, p. 425–441. [https://doi.org/10.1130/B31335.1]

- Eddy, M. P.; Umhoefer, P. J.; Miller, R. B.; Donaghy, E. E.; Gundersen, Melissa; Senes, F. I., 2017, Sedimentary, volcanic, and structural processes during triple-junction migration: Insights from the Paleogene record in central Washington. *In* Haugerud, R. A.; Kelsey, H. M., editors, *From the Puget Lowland to east of the Cascade Range: Geologic excursions in the Pacific Northwest*: Geological Society of America Field Guide 49, p. 143–174. [https://doi.org/10.1130/2017.0049(07)]
- Emery-Wetherell, M. M.; Schilter, J. F., 2020, A new early occurrence of Cervidae in North America from the Miocene-Pliocene Ellensburg Formation in Washington, USA: *Palaeontologia Electronica*, v. 23, no. 1, 11 p. [https://doi.org/10.26879/946]
- Fields, S. A., 2023, Geochemical investigations into a Miocene/Pliocene tephra which may constrain the timing of Cervidae in North America: University of Houston Senior Honors Thesis, 52 p. [https://uh-ir.tdl.org/server/api/core/bitstreams/5ff4bca8-6f25-42e4-917a-706c863a40d0/content]
- Hammond, P. E., 2013, Distribution, stratigraphy, and structure of the Grande Ronde Basalt in the upper Naches River basin, Yakima and Kittitas Counties, Washington. *In* Reidel, S. P.; Camp, V. E.; Ross, M. E.; Wolff, J. A.; Martin, B. S.; Tolan, T. L.; Wells, R. E., editors, *The Columbia River flood basalt province: Geological Society of America Special Paper 497*, p. 363–400. [https://doi.org/10.1130/2013.2497(15)]
- Heiskanen, W. A.; Vening-Meinesz, F. A., 1958, *The Earth and its gravity field*: McGraw-Hill Book Company, Inc., 470 p.
- Hoyt, C. L., 1961, The Hammond sill—An intrusion in the Yakima Basalt near Wenatchee, Washington: *Northwest Science*, v. 35, no. 2, p. 58–64.
- International Union of Geodesy and Geophysics, 1971, *Geodetic reference system 1967*: International Association of Geodesy Special Publication no. 3, 116 p.
- Johnson, S. Y., 1985, Eocene strike-slip faulting and nonmarine basin formation in Washington. *In* Biddle, K. T.; Christie-Blick, Nicholas, editors, *Strike-Slip Deformation, Basin Formation, and Sedimentation*: Society of Economic Paleontologists and Mineralogists Society for Sedimentary Geology Special Publication 37, p. 283–302. [https://doi.org/10.2110/pec.85.37.0265]
- Jones, M. A.; Vaccaro, J. J.; Watkins, A. M., 2006, Hydrogeologic framework of sedimentary deposits in six structural basins, Yakima River basin, Washington: U.S. Geological Survey Scientific Investigations Report 2006-5116, 24 p. [https://pubs.usgs.gov/sir/2006/5116/]
- Jones, M. A.; Vaccaro, J. J., 2008, Extent and depth to top of basalt and interbed hydrogeologic units, Yakima River basin aquifer system, Washington: U.S. Geological Survey Scientific Investigations Report 2008-5045, 22 p., 5 plates. [https://pubs.usgs.gov/sir/2008/5045/]
- Kaatz, M. R., 1959, Patterned ground in central Washington: A preliminary report: *Northwest Science*, v. 33, no. 4, p. 145–156.
- Kasbohm, Jennifer; Schoene, Blair, 2018, Rapid eruption of the Columbia River flood basalt and correlation with the mid-Miocene climate optimum: *Science Advances*, v. 4, no. 9. [https://doi.org/10.1126/sciadv.aat8223]
- Kasbohm, Jennifer; Schoene, Blair; Mark, D. F.; Murray, Joshua; Reidel, Stephen; Szymanowski, Dawid; Barfod, Dan; Barry, Tiffany, 2023, Eruption history of the Columbia River Basalt Group constrained by high-precision U-Pb and ⁴⁰Ar/³⁹Ar geochronology: *Earth and Planetary Science Letters*, v. 617. [https://doi.org/10.1016/j.epsl.2023.118269]
- Kelsey, H. M.; Ladinsky, T. C.; Staisch, Lydia; Sherrod, B. L.; Blakely, R. J.; Pratt, T. L.; Stephenson, W. J.; Odum, J. K.; Wan, Elmira, 2017, The Story of a Yakima fold and how it informs late Neogene and Quaternary backarc deformation in the Cascadia subduction zone, Manastash anticline, Washington, USA: *Tectonics*, v. 36, no. 10, p. 2,085–2,107. [https://doi.org/10.1002/2017TC004558]
- Ladinsky, T. C., 2012, Late Quaternary evolution of the Manastash anticline and Manastash range front, Yakima fold belt, Washington— influence of tectonics and climate: California State Polytechnic University, Humboldt, Master of Science thesis, 85 p. [https://scholarworks.calstate.edu/downloads/h128nh254]
- Ladinsky, T. C.; Kelsey, H. M., 2012, Late Quaternary landscape evolution and deformation in the forelimb region of the Manastash anticline, Yakima fold belt, Washington: U.S. Geological Survey National Earthquake Hazards Reduction Program Final Technical Report, 39 p. [https://earthquake.usgs.gov/cfusion/external_grants/reports/G10AC00686.pdf]
- Lamb, Jodie, 1997, Quaternary stratigraphy of the Kittitas Valley, with emphasis on the Craigs Hill section: Central Washington University undergraduate thesis, 96 p.
- Lanphere, M. A.; Baadsgaard, Halfdan, 2001, Precise K–Ar, ⁴⁰Ar/³⁹Ar, Rb–Sr and U/Pb mineral ages from the 27.5 Ma Fish Canyon Tuff reference standard: *Chemical Geology*, v. 175, no. 3–4, p. 653–671. [https://doi.org/10.1016/S0009-2541(00)00291-6]
- Li, Tao; Chen, Jie; Thompson Jobe, J. A.; Burbank, D. W., 2017, Active flexural-slip faulting: Controls exerted by stratigraphy, geometry, and fold kinematics: *Journal of Geophysical Research: Solid Earth*, v. 122, no. 10, p. 8,538–8,565. [https://doi.org/10.1002/2017JB013966]
- Li, Tao; Chen, Jie; Thompson Jobe, J. A.; Burbank, D. W.; Cheng, Xiaogan; Xu, Jianhong; Li, Zhigang; Zheng, Wenjun; Zhang, Peizhen, 2018, Active bending-moment faulting: Geomorphic expression, controlling conditions, accommodation of fold deformation: *Tectonics*, v. 37, no. 8, p. 2,278–2,306. [https://doi.org/10.1029/2018TC004982]
- Ludwig, K. R., 2012, *Isoplot 4.16: A geochronological toolkit for Microsoft Excel*: Berkeley Geochronological Center Special Publication no. 5, 75 p.
- Martin, B. S., 1989, The Roza Member, Columbia River Basalt Group: Chemical stratigraphy and flow distribution. *In* Reidel, S. P.; Hooper, P. R., editors, *Volcanism and tectonism in the Columbia River flood-basalt province: Geological Society of America Special Paper 239*, p. 85–104. [https://doi.org/10.1130/SPE239-p85]
- Martin, B. S.; Tolan, T. L.; Reidel, S. P., 2013, Revisions to the stratigraphy and distribution of the Frenchman Springs Member, Wanapum Basalt. *In* Reidel, S. P.; Camp, V. E.; Ross, M. E.; Wolff, J. A.; Martin, B. S.; Tolan, T. L.; Wells, R. E., editors, *The Columbia River Flood Basalt Province: Geological Society of America Special Paper 497*, p. 155–180. [https://doi.org/10.1130/2013.2497(06)]
- McCaffrey, Robert; King, R. W.; Payne, S. J.; Lancaster, Matthew, 2013, Active tectonics of northwestern U. S. inferred from GPS-derived surface velocities: *Journal of Geophysical Research Solid Earth*, v. 118, no. 2, p. 709–723. [https://doi.org/10.1029/2012JB009473]
- McDonald, E. V.; Busacca, A. J., 1992, Late Quaternary stratigraphy of loess in the Channeled Scabland and Palouse regions of Washington State: *Quaternary Research*, v. 38, no. 2, p. 141–156. [https://doi.org/10.1016/0033-5894(92)90052-K]
- McMillan, Kent; Long, P. E.; Cross, R. W., 1989, Vesiculation in Columbia River Basalts. *In* Reidel, S. P.; Hooper, P. R., editors, *Volcanism and Tectonism in the Columbia River Flood-Basalt Province: Geological Society of America Special Paper 239*, p. 157–167. [https://doi.org/10.1130/SPE239-p157]
- Mitra, Shankar, 2002, Fold-accommodation faults: *AAPG Bulletin*, v. 86, no. 4, p. 671–693. [https://doi.org/10.1306/61EEDB7A-173E-11D7-8645000102C1865D]
- Morelli, Carlo; Gantar, C.; Honkasalo, Tauno; McConnel, R. K.; Tanner, J. G.; Szabo, Bela; Uotila, Urho; Whalen, C. T., 1974, *The international gravity standardization net 1971 (I.G.S.N.71)*: International Association of Geodesy Special Publication No. 4, 194 p. [https://apps.dtic.mil/sti/citations/ADA006203]
- Mustoe, G. E., 2023, Silicification of wood: An overview: *Minerals*, v. 12, no. 2. [https://doi.org/10.3390/min13020206]

- Myers, Ellie, 2019, The age and origin of soil mounds on Manastash Ridge in Kittitas County, Washington: Central Washington University Undergraduate Thesis, 61 p. [<https://www.gis.cwu.edu/geog/documents/Myers-2019-Age-Origin-Soil-Mound-Manastash-Ridge.pdf>]
- Nilsen, T. H., 1976, Washington gravity base station network: Washington Division of Geology and Earth Resources Information Circular 59, 83 p. [https://www.dnr.wa.gov/Publications/ger_ic59_wa_gravity_base_network.pdf]
- O'Connor, J. E.; Wells, R. E.; Bennett, S. E. K.; Cannon, C. M.; Staisch, L. M.; Anderson, J. L.; Pivarunas, A. F.; Gordon, G. W.; Blakely, R. J.; Stelten, M. E.; Everts, R. C., 2021, Arc versus river—The geology of the Columbia River gorge. *In* Booth, A. M.; Grunder, A. L., editors, From terranes to terrains: Geologic field guides on the construction and destruction of the Pacific Northwest: Geological Society of America Field Guide 62, p. 131–186. [[https://doi.org/10.1130/2021.0062\(05\)](https://doi.org/10.1130/2021.0062(05))]
- Paces, J. B.; Miller, J. D., Jr., 1993, Precise U-Pb ages of Duluth Complex and related mafic intrusions, northeastern Minnesota: Geochronological insights to physical, petrogenetic, paleomagnetic, and tectonomagmatic processes associated with the 1.1 Ga Midcontinent Rift System: *Journal of Geophysical Research*, v. 98, no. B8, p. 13,997–14,013. [<https://doi.org/10.1029/93JB01159>]
- Paton, Chad; Hellstrom, John; Paul, Bence; Woodhead, Jon; Hergt, Janet, 2011, Iolite: Freeware for the visualization and processing of mass spectrometric data: *Journal of Analytical Atomic Spectrometry*, v. 26, p. 2,508–2,518. [<https://doi.org/10.1039/C1JA10172B>]
- Phillips, J. D.; Hansen, R. O.; Blakely, R. J., 2007, The use of curvature in potential-field interpretation: *Exploration Geophysics*, v. 38, p. 111–119. [<https://doi.org/10.1071/EG07014>]
- Plouff, Donald, 2000, Field estimates of gravity terrain corrections and Y2K-compatible method to convert from gravity readings with multiple base stations to tide- and long-term drift-corrected observations: U.S. Geological Survey Open-File Report 00-140, 37 p. [<https://pubs.usgs.gov/of/2000/0140/>]
- Porter, S. C., 1976, Pleistocene glaciation in the southern part of the north Cascade Range, Washington: *Geological Society of America Bulletin*, v. 87, no. 1, p. 61–75. [[https://doi.org/10.1130/0016-7606\(1976\)87<61:PGITSP>2.0.CO;2](https://doi.org/10.1130/0016-7606(1976)87<61:PGITSP>2.0.CO;2)]
- Reidel, S. P.; Scott, G. R.; Bazard, D. R.; Cross, R. W.; Dick, Brian, 1984, Post-12 million year clockwise rotation in the central Columbia Plateau, Washington: *Tectonics*, v. 3, no. 2, p. 251–273. [<https://doi.org/10.1029/TC003i002p00251>]
- Reidel, S. P.; Fecht, K. R.; Hagood, M. C.; Tolan, T. L., 1989, The geologic evolution of the central Columbia Plateau. *In* Reidel, S. P.; Hooper, P. R., editors, Volcanism and tectonism in the Columbia River flood-basalt province: Geological Society of America Special Paper 239, p. 247–264. [<https://doi.org/10.1130/SPE239-p247>]
- Reidel, S. P., 2005, A Lava Flow without a Source: The Cohasset flow and its compositional components, Sentinel Bluffs Member, Columbia River Basalt Group: *Journal of Geology*, v. 113, no. 1, p. 1–21. [<https://doi.org/10.1086/425966>]
- Reidel, S. P.; Tolan, T. L., 2013a, The Grande Ronde Basalt, Columbia River Basalt Group. *In* Reidel, S. P.; Camp, V. E.; Ross, M. E.; Wolff, J. A.; Martin, B. S.; Tolan, T. L.; Wells, R. E., editors, The Columbia River flood-basalt province: Geological Society of America Special Paper 497, p. 117–154. [[https://doi.org/10.1130/2013.2497\(05\)](https://doi.org/10.1130/2013.2497(05))]
- Reidel, S. P.; Tolan, T. L., 2013b, The late Cenozoic evolution of the Columbia River system in the Columbia River flood-basalt province. *In* Reidel, S. P.; Tolan, T. L.; Camp, V. E.; Ross, M. E.; Wolff, J. A.; Martin, B. S.; Wells, R. E., editors, The Columbia River flood-basalt province: Geological Society of America Special Paper 497, p. 201–230. [[https://doi.org/10.1130/2013.2497\(08\)](https://doi.org/10.1130/2013.2497(08))]
- Reidel, S. P.; Camp, V. E.; Tolan, T. L.; Martin, B. S., 2013a, The Columbia River flood-basalt province: Stratigraphy, areal extent, volume, and physical volcanology. *In* Reidel, S. P.; Camp, V. E.; Ross, M. E.; Wolff, J. A.; Martin, B. S.; Tolan, T. L.; Wells, R. E., editors, The Columbia River flood-basalt province: Geological Society of America Special Paper 497, p. 1–44. [[https://doi.org/10.1130/2013.2497\(01\)](https://doi.org/10.1130/2013.2497(01))]
- Reidel, S. P.; Camp, V. E.; Tolan, T. L.; Kauffman, J. D.; Garwood, D. L., 2013b, Tectonic evolution of the Columbia River flood-basalt province. *In* Reidel, S. P.; Camp, V. E.; Ross, M. E.; Wolff, J. A.; Martin, B. S.; Tolan, T. L.; Wells, R. E., editors, The Columbia River flood-basalt province: Geological Society of America Special Paper 497, p. 293–324. [[https://doi.org/10.1130/2013.2497\(12\)](https://doi.org/10.1130/2013.2497(12))]
- Reidel, S. P.; Camp, V. E.; Ross, M. E.; Wolff, J. A.; Martin, B. S.; Tolan, T. L.; Wells, R. E., editors, 2013c, The Columbia River flood-basalt province: Geological Society of America Special Paper 497, 440 p. [<https://doi.org/10.1130/SPE497>]
- Reidel, S. P., 2015, Igneous rock associations 15. The Columbia River Basalt Group: A flood-basalt province in the Pacific Northwest, USA: *Geoscience Canada*, v. 42, no. 1, p. 151–168. [<https://id.erudit.org/iderudit/1029230ar>]
- Reidel, S. P.; Hooper, P. R., editors, Volcanism and tectonism in the Columbia River flood-basalt province: Geological Society of America Special Paper 239, 386 p. [<https://doi.org/10.1130/SPE239>]
- Rosenmeier, F. J., 1968, Stratigraphy and structure of the Table Mountain–Mission Peak area in the Wenatchee Mountains, central Washington: University of Washington Master of Science thesis, 44 p., 1 plate.
- Sadowski, A. J.; McCosby, J. B.; Anderson, M. L.; Lau, T. R.; Steiner, Ashley; DuFrane, S. A.; Rittenour, Tammy; Housen, Bernard, 2020, Geologic map of the Ellensburg North and southern half of the Reecer Canyon 7.5-minute quadrangles, Kittitas County, Washington: Washington Geological Survey Map Series 2020-01, 1 sheet, scale 1:24,000, 25 p. text. [https://www.dnr.wa.gov/publications/ger_ms2020-01_geol_map_ellensburg_north_reecer_canyon_24k.zip]
- Sadowski, A. J.; Gilliland, A. L.; Anderson, M. L., 2021, Geologic map of the Colockum Pass SW and southern half of the Naneum Canyon 7.5-minute quadrangles, Kittitas County, Washington: Washington Geological Survey Map Series 2021-03, 1 sheet, scale 1:24,000, 23 p. text. [https://www.dnr.wa.gov/publications/ger_ms2021-03_geol_map_colockum_pass_sw_southern_naneum_canyon_24k.zip]
- Sadowski, A. J.; Lau, T. R., 2022, Geologic map of the Colockum Pass SE 7.5-minute quadrangle, Kittitas County, Washington: Washington Geological Survey Map Series 2022-05, 1 sheet, scale 1:24,000, 21 p. text. [https://www.dnr.wa.gov/publications/ger_ms2022-05_geol_map_colockum_pass_se_24k.zip]
- Sadowski, A. J.; Wetherell, L. R.; Anderson, M. L.; Powell, J. E., 2023, Geologic map of the Kittitas and East Kittitas 7.5-minute quadrangles, Kittitas County, Washington: Washington Geological Survey Map Series 2023-05, 1 sheet, scale 1:24,000, with 32 p. text. [https://www.dnr.wa.gov/publications/ger_ms2023-05_geol_map_kittitas_e_kittitas_24k.zip]
- Sawlan, M. G., 2018, Alteration, mass analysis, and magmatic composition of the Sentinel Bluffs Member, Columbia River flood-basalt province: *Geosphere*, v. 14, no. 1, p. 286–303. [<https://doi.org/10.1130/GES01188.1>]
- Schmincke, Hans-Ulrich, 1964, Petrology, paleocurrents, and stratigraphy of the Ellensburg Formation and interbedded Yakima Basalt flows, south-central Washington: Johns Hopkins University Doctor of Philosophy thesis, 426 p. [<https://www.proquest.com/openview/e0dede73b99d767153aac7e9c7afc13e/1.pdf?pq-origsite=gscholar&cbl=18750&diss=y>]

- Schmincke, Hans-Ulrich, 1967a, Stratigraphy and petrography of four upper Yakima basalt flows in south-central Washington, v. 78, no. 11, p. 1,385–1,422. [https://doi.org/10.1130/0016-7606(1967)78[1385:SAPOFU]2.0.CO;2]
- Schmincke, Hans-Ulrich, 1967b, Graded lahars in the type sections of the Ellensburg Formation, south-central Washington: *Journal of Sedimentary Research*, v. 37, no. 2, p. 438–448. [https://doi.org/10.1306/74D716EA-2B21-11D7-8648000102C1865D]
- Schuster, J. E., compiler, 1994, Geologic map of the east half of the Yakima 1:100,000 quadrangle, Washington: Washington Division of Geology and Earth Resources Open File Report 94-12, 19 p., 1 plate. [https://www.dnr.wa.gov/Publications/ger_ofr94-12_geol_map_yakima_e_100k.zip]
- Sláma, Jiří; Košler, Jan; Condon, D. J.; Crowley, J. L.; Gerdes, Alex; Hanchar, J. M.; Horstwood, M. S. A.; Morris, G. A.; Nasdala, Lutz; Norberg, Nicholas; Schaltegger, Urs; Schoene, Blair; Tubrett, M. N.; Whitehouse, M. J., 2008, Plešovice zircon—A new natural reference material for U-Pb and Hf isotopic microanalysis: *Chemical Geology*, v. 249, no. 1–2, p. 1–35. [https://doi.org/10.1016/j.chemgeo.2007.11.005]
- Smith, G. O., 1903a, Geologic atlas of the United States—Ellensburg folio, Washington: U.S. Geological Survey Geologic Folio 86, 7 p., with 3 maps, scale 1:125,000. [https://doi.org/10.3133/gf86]
- Smith, G. O., 1903b, Anticlinal mountain ridges in central Washington: *Journal of Geology*, v. 11, no. 2, p. 166–177. [https://www.journals.uchicago.edu/doi/pdf/10.1086/621067]
- Smith, G. A., 1988a, Neogene synvolcanic and syntectonic sedimentation in central Washington: *Geological Society of America Bulletin*, v. 100, no. 9, p. 1,479–1,492. [https://doi.org/10.1130/0016-7606(1988)100<1479:NSASSI>2.3.CO;2]
- Smith, G. A., 1988b, Sedimentology of proximal to distal volcanics dispersed across an active foldbelt: Ellensburg Formation (late Miocene), central Washington: *Sedimentology*, v. 35, no. 6, p. 953–977. [https://doi.org/10.1111/j.1365-3091.1988.tb01740.x]
- Smith, G. A., Shafiqullah, Muhammad; Campbell, N. P.; Deacon, M. W., 1989, Geochronology of the Ellensburg Formation—constraints on Neogene volcanism and stratigraphic relationships in central Washington: *Isochron/West*, *Bulletin of Isotopic Geochronology*, v. 53, p. 28–32. [https://geoinfo.nmt.edu/publications/periodicals/isochronwest/53/IW_v53_p28.pdf]
- Staisch, Lydia; Blakely, Richard; Kelsey, Harvey; Styron, Richard; Sherrod, Brian, 2018a, Crustal structure and Quaternary acceleration of deformation rates in central Washington revealed by stream profile inversion, potential field geophysics, and structural geology of the Yakima folds: *Tectonics*, v. 37, no. 6, p. 1,750–1,770. [https://doi.org/10.1029/2017TC004916]
- Staisch, Lydia; Kelsey, Harvey; Sherrod, Brian; Moller, Andreas; Paces, James; Blakely, Richard; Styron, Richard, 2018b, Miocene–Pleistocene deformation of the Saddle Mountains: Implications for seismic hazard in central Washington, USA: *Geological Society of America Bulletin*, v. 130, no. 3–4, p. 411–437. [https://doi.org/10.1130/B31783.1]
- Staisch, L. M.; Holm-Denoma, C. S.; Pianowski, L. S., 2023, U-Pb zircon data for volcanic and sedimentary units within the Kittitas Valley, central Washington State: U.S. Geological Survey Data Release. [https://doi.org/10.5066/P970M1LW]
- Staley, A. E., 2015, Glacial geomorphology and chronology of the Quinault Valley, Washington, and broader evidence of marine isotope stages 4 and 3 glaciation across northwestern United States: Idaho State University Master of Science thesis, 177 p. [https://etd.iri.isu.edu/ViewSpecimen.aspx?ID=247]
- Swanson, D. A.; Wright, T. L., 1976, Guide to field trip between Pasco and Pullman, Washington, emphasizing stratigraphy, vent areas, and intracanyon flows of Yakima Basalt; Geological Society of America Cordilleran Section, 72nd Annual Meeting, Field guide no. 1: Washington State University Department of Geology, 33 p. [https://s3.wp.wsu.edu/uploads/sites/2191/2017/02/guide-to-field-trip-between-pasco-and-pullman-wa.pdf]
- Swanson, D. A.; Wright, T. L., 1978, Bedrock geology of the northern Columbia Plateau and adjacent areas. In Baker, V. R.; Nummedal, Dag, editors, *The channeled scablands—A guide to the geomorphology of the Columbia Basin*, Washington: U.S. National Aeronautics and Space Administration, p. 37–57. [https://core.ac.uk/download/pdf/42873545.pdf]
- Swick, C. H., 1942, Pendulum gravity measurements and isostatic reductions: U.S. Department of Commerce Coast and Geodetic Survey Special Publication 232, 82 p.
- Sweeney, M. R.; McDonald, E. V.; Gaylord, D. R., 2017, Generation of the Palouse loess: Exploring the linkages between glaciation, outburst megafloods, and eolian deposition in Washington State. In Haugerud, R. A.; Kelsey, H. M., editors, *From the Puget Lowland to East of the Cascade Range: Geologic Excursions in the Pacific Northwest: Geological Society of America Field Guide 49*, p. 207–228. [https://www.doi.org/10.1130/2017.0049(09)]
- Tabor, R. W.; Waitt, R. B., Jr.; Frizzell, V. A., Jr.; Swanson, D. A.; Byerly, G. R.; Bentley, R. D., 1982, Geologic map of the Wenatchee 1:100,000 quadrangle, central Washington: U.S. Geological Survey Miscellaneous Investigations Series Map I-1311, 1 sheet, scale 1:100,000, with 26 p. text. [https://doi.org/10.3133/i1311]
- Tavani, Stefano; Storti, F.; Lacombe, O.; Corradetti, A.; Muñoz, J.A.; Mazzoli, S., 2015, A review of deformation pattern templates in foreland basin systems and fold-and-thrust belts: Implications for the state of stress in the frontal regions of thrust wedges: *Earth-Science Reviews*, v. 141, p. 82–104. [https://doi.org/10.1016/j.earscirev.2014.11.013]
- Telford, W. M.; Geldart, L. O.; Sheriff, R. E., 1990, *Applied Geophysics*: New York, Cambridge University Press, 770 p.
- Thackray, G. D., 2001, Extensive early and middle Wisconsin glaciation on the western Olympic Peninsula, Washington, and the variability of Pacific moisture delivery to the northwestern United States: *Quaternary Research*, v. 55, no. 3, p. 257–270. [https://doi.org/10.1006/qres.2001.2220]
- Tolan, T. L.; Reidel, S. P.; Beeson, M. H.; Anderson, J. L.; Fecht, K. R.; Swanson, D. A., 1989, Revisions to the estimates of the areal extent and volume of the Columbia River Basalt Group. In Reidel, S. P.; Hooper, P. R., editors, *Volcanism and tectonism in the Columbia River flood-basalt province: Geological Society of America Special Paper 239*, p. 1–20. [https://doi.org/10.1130/SPE239-pl]
- Vaccaro, J. J.; Jones, M. A.; Ely, D. M.; Keys, M. E.; Olsen, T. D.; Welch, W. B.; Cox, S. E., 2009, Hydrogeologic framework of the Yakima River basin aquifer system, Washington: U.S. Geological Survey Scientific Investigations Report 2009-5152, 106 p. [https://pubs.usgs.gov/sir/2009/5152/]
- Vermeesch, Pieter, 2018, IsoplotR: a free and open toolbox for geochronology: *Geoscience Frontiers*, v. 9, p. 1,479–1,493. [https://doi.org/10.1016/j.gsf.2018.04.001]
- Vermeesch, Pieter, 2021, Maximum depositional age estimation revisited: *Geoscience Frontiers*, v. 12, no. 2, p. 843–850. [https://doi.org/10.1016/j.gsf.2020.08.008]
- Waitt, R. B., Jr., 1979, Late Cenozoic deposits, landforms, stratigraphy, and tectonism in Kittitas Valley, Washington: U.S. Geological Survey Professional Paper 1127, 18 p. [https://doi.org/10.3133/pp1127]
- Washington Geological Survey, 2018, Yakima Basin 2018 project [lidar data]: originally contracted by Washington Dept. of Natural Resources. [accessed May 2023, at https://lidarportal.dnr.wa.gov/]

- Washington Geological Survey, 2022, East Cascades South 2020 project [lidar data]: originally contracted by Washington Dept. of Natural Resources and U.S. Geological Survey. [accessed May 2023, at <https://lidarportal.dnr.wa.gov/>]
- Wells, R. E.; Weaver, C. S.; Blakely, R. J., 1998, Fore-arc migration in Cascadia and its neotectonic significance: *Geology*, v. 26, no. 8, p. 759–762. [[https://doi.org/10.1130/0091-7613\(1998\)026<0759:FAMICA>2.3.CO;2](https://doi.org/10.1130/0091-7613(1998)026<0759:FAMICA>2.3.CO;2)]
- Wells, R. E.; McCaffrey, Robert, 2013, Steady rotation of the Cascade arc: *Geology*, v. 41, no. 9, p. 1,027–1,030. [<https://doi.org/10.1130/G34514.1>]
- Whitlock, Cathy; Sarna-Wojcicki, A. M.; Bartlein, P. J.; Nickmann, R. J., 2000, Environmental history and tephrostratigraphy at Carp Lake, southwestern Columbia Basin, Washington, USA: *Palaeogeography, Palaeoclimatology, Palaeoecology*, v. 155, p. 7–29. [[https://doi.org/10.1016/S0031-0182\(99\)00092-9](https://doi.org/10.1016/S0031-0182(99)00092-9)]
- Wiedenbeck, Michael; Allé, P.; Corfu, Fernando; Griffin, W. L.; Meier, Martin; Oberli, Felix; Von Quadt, Albrecht; Roddick, J. C.; Spiegel, W., 1995, Three natural zircon standards for U-Th-Pb, Lu-Hf, trace element and REE analyses: *Geostandards Newsletters*, v. 19, p. 1–23. [<https://doi.org/10.1111/j.1751-908X.1995.tb00147.x>]
- Williams, I. S., 1998, U-Th-Pb geochronology by ion microprobe. *In* McKibben, M. A.; Shanks, W.C., III; Ridley, W.I., editors, *Applications of microanalytical techniques to understanding mineralizing processes: Reviews in Economic Geology*, v. 7, p. 1–35. [<https://doi.org/10.5382/Rev.07>]
- Williams, Howel; Masson, P. H., 1949, *Geology of the Macdoel quadrangle, with a section on circular soil structures in northeastern California*: California Division of Mines and Geology, Bulletin 151, scale 1:125,000. [https://ngmdb.usgs.gov/Prodesc/proddesc_531.htm]
- Woodring, D. N., 2020, Kinematics of the Columbia Hills anticline and the Warwick strike-slip fault, Yakima fold and thrust belt, Washington, USA: Oregon State University Master of Science thesis, 108 p., 1 plate.

Appendix A. Gravity

OVERVIEW

Lateral changes in isostatic gravity across a region result from density changes within rocks of the mid to upper crust. Gravity surveys are especially useful in delineating steeply dipping contacts between two rock bodies with contrasting density. The goals of the gravity survey conducted for this study are to: (1) delineate position and geometry of density contrasts within the subsurface, (2) determine length and geometry of known structures, and (3) identify previously unknown structures.

DATA ACQUISITION

New gravity measurements (stations) from 243 individual points collected using a Scintrex CG-6 meter (Serial # 19050174) supplement 1,200 stations from previous studies (Sadowski and others, 2020, 2021, 2022) and 5 stations from the PACES database (now defunct; data obtained from B. Drenth, U. S. Geological Survey, written commun., 2020). We used the the Ellensburg B base station (Nilsen, 1976) to tie our data to the U.S. gravity network. Gravity station spacing at roughly 2 km generated a basic grid over a large area, while denser 1-km spacing was used in areas where known structures exist or where initial gravity data collection showed a significant gradient. Along modeled cross section lines, station spacing was roughly 250 m, as access allowed. A Javad Triumph-2 differential GPS unit provided the horizontal and vertical position of each station wherever we didn't use LiDAR for the same positional information.

DATA CORRECTIONS AND PROCESSING

The proprietary Javad Justin software allows for post-processing to make differential corrections utilizing NOAA and the National Geodetic Survey's Continuously Operating Reference Stations (CORS) within 70 km of the study area. After processing, typical positional accuracy is 0.15 m in the vertical and horizontal. Where lidar-based elevations are likely higher precision than GPS elevations, we use them in our analysis. We apply the factory gravimeter calibration constants to each gravity observation, apply correction factors obtained from the Mount Hamilton calibration loop east of San Jose, CA (Barnes and others, 1969), and correct for Earth tides to produce observed gravity values. The data reference the International Gravity Standardization Net of 1971 (Morelli, 1974), and the reference ellipsoid is the Geodetic Reference System of 1967 (International Association of Geodesy and Geophysics, 1971). The assumed linear drift between base-station ties results in a maximum gravity reading error of 0.005 mGal.

Gravity data reduction formulas for the free-air anomaly are standard (for example, Telford and others, 1990; Swick, 1942) and we applied Bouguer, Earth curvature, and terrain corrections out to 166.7 km from each station to produce a complete Bouguer anomaly. Terrain corrections are a combination of a field-based component (to a radius of 68 m using the Hayford system; Plouff, 2000) and a computer-generated component (using 30-m USGS DEM grids). The complete Bouguer anomaly is further reduced to an isostatic anomaly using an Airy-Heiskanen model (Heiskanen and Vening-Meinesz, 1958), assuming a 25-km-thick crust at sea level and a crust-mantle density contrast of 400 kg/m³. All parts of the data-reduction process assume a standard reduction density of 2,670 kg/m³. Gravity readings and computed anomalies are in the Data Supplement.

Gravity data uncertainties are predominantly due to imprecise vertical position and terrain correction uncertainty. Average gravity value error from elevation uncertainty is 0.03 mGal. The uncertainty associated with terrain corrections is generally only 5–10 percent of the actual correction. Average uncertainty in steep and hilly regions is 0.12–0.23 mGal, whereas average uncertainty in flatter areas is 0.05–0.1 mGal. Based on these uncertainties, we can interpret gravity anomalies of 0.5–1 mGal or greater in terms of density variations in the upper crust.

The minimum curvature algorithms in the GIS software package Geosoft Oasis Montaj (Seequent, Inc.) transform our point isostatic anomaly data into gridded surfaces, which we use to produce 0.5 mGal contours (Fig. M1A). The maximum horizontal gradients (referred to as 'max-spots'), calculated using the curvature analysis methodology of Phillips and others (2007), quantitatively locate strong and linear boundaries between rocks in the subsurface that have substantial density differences.

Appendix B. Rock Physical Properties

OVERVIEW

Measurements of rock density and magnetic susceptibility from geologic unit samples in our map area constrain our geophysical model parameters (Appendix C). We refer to these collectively as ‘rock properties’ in the text.

DESCRIPTION OF METHOD

We collected 48 bedrock samples throughout the study area for laboratory analysis. We weighed samples using an A&D company limited FX-3000i WP analytical balance. Three measurements per sample combine to determine density: a dry weight in air, a submerged (water-saturated) weight, and a water-saturated weight in air. While these measurements produce grain density, saturated bulk density, and dry bulk density, saturated bulk density best reflects subsurface conditions and was therefore referenced for modeling. Magnetic susceptibility measurements taken with a KT10 Kappa Meter accompany rock sample density measurements, and we use the same meter to collect direct readings from outcrops where possible. We collected magnetic susceptibility measurements from 18 additional outcrops that we did not sample. In outcrops, weathering tends to replace denser minerals with less dense weathering products, such as conversion of magnetite into hematite. Therefore, all our measured rock densities and susceptibilities from surface outcrops (see Data Supplement) can be considered minimum values. While we do not directly measure magnetic remanence in the field or from samples, we do use magnetic remanence values in our models by referring to published values when available.

Appendix C. Quantitative Geophysical Modeling of Geologic Cross Sections

OVERVIEW

Quantitative two-dimensional forward modeling of cross sections constrained by potential-field data, well logs, and surficial geologic observations provides more insight into subsurface geology than qualitative interpretations based only on surficial geologic observations. Subsurface modeling helps provide the best possible interpretation of fault type (for example normal, reverse, or strike-slip), fault dip, and offset across the fault on units with particularly strong physical-property contrasts with surrounding rocks. This method also can identify blind faults that have little surface expression and are difficult to capture via surface geology observations.

DESCRIPTION OF METHOD

GM-SYS (provided with the Oasis-Montaj GIS software, Seequent, Inc.) computes the magnetic and gravitational fields produced by two-dimensional configurations of rock in the subsurface. This is a forward-modeling method wherein the operator hypothesizes the locations, extents, and volumes of rock types with specified physical properties in the subsurface. The GM-SYS program predicts the gravitational and magnetic fields that result from each particular rock configuration. The operator refines the subsurface rock configuration until the modeled potential fields approach or match observed potential fields.

We start with initial simplified models, including uniform packages of sediment, sedimentary rock, metamorphic rock, or volcanic rock to fit the overall long-wavelength features in the gravity and magnetic data. Our model space extends beyond the end of modeled cross sections to avoid edge effects due to truncated subsurface volumes. Incrementally adding detail to our modeled stratigraphy by adjusting depths of geologic contacts, adding or removing geologic structures, and even inserting intrusions while progressively decreasing the size of model blocks allows us to fit long-wavelength anomalies first in the deeper subsurface (produced by larger-scale features deeper in the subsurface) and to then fit short-wavelength anomalies, mainly produced by smaller-scale features near the surface.

Constraints on our geophysical modeling include surface geologic observations that define the lithologies that constrain the model's surficial and near-surface parameters. Surface geologic observations also define the geologic relationships among probable stratigraphy we expect in the deeper subsurface. Reasonable structural geometries are informed by geologic mapping and standard models for cross-section construction to provide additional constraint. Lab measurements (Appendix B) of density and magnetic properties of hand samples gathered from the surface provide approximate rock properties for the purposes of modeling. Applying these geologic constraints limits plausible subsurface rock geometries. We show best-fit geophysical models for each geologic cross section on the Map Sheet.

Even within these constraints, subsurface solutions to the gravity and magnetic data may be non-unique. In general, potential-field data provide strong constraints on the position and dip of simple, steeply dipping boundaries that juxtapose rocks with strong differences in physical properties. Potential-field data provide a poor constraint on horizontal boundaries or on boundaries between rocks with little contrast in physical properties. Depth of sub-horizontal stratigraphic boundaries within sedimentary rocks is not well constrained by potential-field data, but good quality well or seismic-reflection data inform subsurface model geometries.

Appendix D. Geochemistry

OVERVIEW

We analyzed major and trace element composition of volcanic rocks in the map area using X-Ray Fluorescence (XRF) on whole rock samples. This method allows us to determine rock elemental compositions and chemostratigraphic classifications. The results of the analyses are presented in the Data Supplement.

SAMPLE COLLECTION AND PREPARATION

We collected 326 samples within, south, and east of the map area, representing a variety of CRBG textures including colonnade, entablature, vesicular tops, hyaloclastite, platy entablature, and autobreccia. We focused on collecting samples from colonnade and entablature because they exhibit less pervasive chemical alteration, and analyses of less altered samples produce more representative geochemical results. However, we collected from the other textures where we had no better outcrop options. We rarely collected samples containing secondary minerals filling veinlets, vugs, or vesicles.

The freshest available samples were collected from outcrops with a sledgehammer. All samples were field cleaned (knapped by hand or using local bedrock exposures as anvils). Weathering rinds were removed as much as possible in the field (>90% of samples). Additional weathering rind cleaning or sample splitting (<10% of samples) was performed at the CWU rock preparation lab using a sledgehammer and steel plate. Removing weathering rinds—if present—from vesicular tops was not always possible. Samples contain varied amounts of weathering, hydration seams, and (or) alteration. Weathered, hydrated, or altered samples were collected and analyzed where no fresher samples were available. In general, samples submitted to the lab ranged in size from centimeter-sized chips to fist-sized fragments.

Hydration seams (“alteration seams”, as described in supplemental file 3 of Sawlan, 2018) were generally avoided but not rigorously removed before sending to WSU for further preparation: crushing, pulverization/powdering, and glass-bead fusion. Laboratory-based sub-sampling (Sawlan, 2018) was not performed due to time constraints. However, we categorize most of our samples into inter-rind to inter-seam sample quality according to table S1 of Sawlan (2018).

DATA CORRECTIONS AND PROCESSING

We used the machine learning (ML) model developed by Dr. Ashley Steiner at the WSU Peter Hooper GeoAnalytical Lab to categorize formations, GRB members, and submembers without stratigraphic context. Overall, the model more confidently distinguishes formation-level units from each other (for example, Wanapum versus Grande Ronde) than member-level or submember-level units from each other. For this reason, we relied less on the ML model for member-level and submember-level classifications compared to previous years. Instead, we plotted elemental variation diagrams (TiO_2 vs. MgO , TiO_2 vs. P_2O_5 , TiO_2 vs. Zr , and Cr), compared sample results to diagrams in Reidel (2005), and used stratigraphy to determine the most reasonable member and submember classifications, especially when ML classifications had low confidence values.

RESULTS

Results for 326 samples are in the Data Supplement. Limits of Determination (LOD) are also included in the column header for each respective analyte in the Data Supplement.

Appendix E. Geochronology

URANIUM-LEAD DATING OF DETRITAL ZIRCONS

Overview

We analyzed sedimentary material in the map area (1) to determine maximum depositional ages (MDAs) and (2) to conduct preliminary assessments of detrital zircon age spectra. We used the Maximum Likelihood Age (MLA) algorithm to estimate MDAs from U-Pb analyses of detrital zircons. We collected samples at two locations. Summary data for these sites are contained in Table E1; individual zircon analytical results are in the Data Supplement.

Sample Collection and Preparation

To understand the depositional ages of units $M_{C_{elc}}$ and $M_{C_{ge}}$, we collected two samples in 2023 for zircon age analysis. We collected ~2–7 kg of fresh rock for each sample, making sure to minimize any contact with soil or other surface deposits, which could introduce zircons from other sources. The packaged samples were sent to ZirChron, LLC for mineral separation. Samples were pressure-washed with water and then disaggregated using an Electro Pulse Disaggregator (EPD, Marx generator) at 1 Hz with discharges of ~250 kV for 15 minutes. Any clasts >500 μm were crushed in a crusher or pulverizer. Using stainless steel sieves, the fraction between 350 μm and 25 μm was retained and then processed using a Wilfley water table, Frantz paramagnetic separator, and a two-step (3.00 g/cm³ and 3.32 g/cm³) heavy liquid methylene iodide mineral density separation. Approximately 100 individual zircon grains from each sample were randomly selected with adhesive tape, mounted in epoxy, polished to expose the grain centers, and regions suitable for analysis were identified from optical imaging. Core regions of detrital grains were analyzed to avoid overgrowths and lead loss, which skew isotopic age calculations.

Analytical Methods

Zircon U-Pb ages were measured at the Radiogenic Isotope and Geochronology Lab (RIGL) at Washington State University using an Analyte G2 193 excimer laser ablation system coupled with a Thermo-Finnigan Element 2 single-collector inductively coupled plasma mass spectrometer. The laser parameters were 25 μm in diameter spot size, 10 Hz repetition rate, and ~5.0 J/cm² fluence. For the U-Pb measurement, we mostly followed the method of Chang and others (2006), except for the use of a 193 nm laser system instead of a 213 nm laser. A 10-second blank measurement of the He and Ar carrier gasses (laser off) before each analysis was followed by 250 scans across masses ²⁰²Hg, ²⁰⁴Pb+²⁰⁴Hg, ²⁰⁶Pb, ²⁰⁷Pb, ²⁰⁸Pb, ²³²Th, ²³⁵U, and ²³⁸U during ~30-second-long laser ablation periods (in other words, one continuous, 30 s ablation at 10 Hz—10 shots fired per second—for ~300 laser shots). Analyses of zircon unknowns, standards, and quality control zircon grains were interspersed with analyses of external calibration standards, typically with 10–12 unknowns bracketed by multiple analyses of two different zircon standards (Plešovice and FC-1). The Plešovice standard (337.13 \pm 0.37 Ma; Sláma and others, 2008) was used to calibrate the ²⁰⁶Pb/²³⁸U and ²⁰⁷Pb/²³⁵U ages, and the FC-1 standard (1,099 Ma; Paces and Miller, 1993) was used for calibration of ²⁰⁷Pb/²⁰⁶Pb ages owing to its high count rate for ²⁰⁷Pb (~2–4 times higher than that of Plešovice). Zircon 91500 (1,065 Ma; Wiedenbeck and others, 1995; n=28, ²⁰⁷Pb/²⁰⁶Pb age=1,063 +2.4/-5.0 Ma), Fish Canyon Tuff (~27.5 Ma; Lanphere and Baadsgaard, 2001; n=35, ²⁰⁶Pb/²³⁸U age=27.9 +0.1/-0.2 Ma) and Temora2 (417 Ma; Black and others, 2004, n=48, ²⁰⁶Pb/²³⁸U age=417.0 \pm 1 Ma) were used as quality control standards. Data were processed offline using the Iolite software (Paton and others, 2011). Common Pb correction was performed using the ²⁰⁷Pb method (Williams, 1998). Plots were generated using Isoplot 4.16 (Ludwig, 2012). Zircon U-Pb analytical data are reported in the Data Supplement.

We analyzed U-Pb isotopic results using two filters in the following order: (1) We omit zircon grains with discordances between -5% and +30%, then (2) by visual inspection of the zircon age spectrum, we included only zircon grains from the youngest peak. Once those grains were removed, the remaining ages were plotted in IsoplotR (Vermeesch, 2018) using a radial diagram with a minimum mixing model to calculate a maximum likelihood age (Vermeesch, 2021), which we report as the MDA.

Results

We report results for samples collected in the summer of 2023. Summary data for our two geochronology sites are contained in Table E1; individual zircon analytical results are in the Data Supplement.

Table E1. U-Pb ages from the Ellensburg South 7.5-minute quadrangle. MDA is 'maximum depositional age.' MLA is maximum likelihood age algorithm of Vermeesch (2021). Full analytical data are available in the Data Supplement.

Site ID	GD01	<p>Analysis of 102 zircon grains from a micaceous sandstone in the eastern portion of the Ellensburg South quadrangle. Sample only contains two Miocene zircons and the youngest single zircon yielded an age of 15.3 ± 0.3 Ma.</p> <p>Age spectrum contains abundant pre-Cenozoic zircons.</p> <p>Sample is from a west-facing outcrop west east of WA State Route 821 (Canyon Road). Exposure is directly overlying the Roza Member and in the core of a faulted syncline. We infer a Miocene age.</p> <p>Sampled 8/2/2023, by A. Sadowski and A. Yokel-Deliduka.</p>
Field sample ID	Ess081	
Map unit	Mcelc	
TRS location	S31 T17N R19E	
Latitude (degrees)	46.91286	
Longitude (degrees)	-120.50566	
Elevation (ft)	1,497	
Age $\pm 2\sigma$		No older than 15.36 ± 0.25 Ma (MDA, calculated using MLA)



Site Photo (photo number 7186). Sample collected from white sandstone (red outline, upper left of photograph) above and left of Roza Member pillow breccia (yellowish brown hyaloclastite, center-right of photograph). Road post is ~1 m tall.

Site ID	GD04	<p>Analysis of 108 zircon grains from loose matrix sand from the conglomerate directly above the most prominent light colored interbed. Sampled at and above the level of paleosol rip up clasts in the western portion of the Ellensburg South quadrangle. The youngest single zircon yielded an age of 9.3 ± 0.4 Ma.</p> <p>Age spectra mostly lacks pre-Cenozoic zircons save only a few Precambrian zircons. The age spectrum also shows a tight cluster of Miocene zircons for a youngest peak, a second large peak in the Paleogene, and broad cluster of Mesozoic zircons.</p> <p>Sample is from a north-facing outcrop on a dirt road (former canal) west of Strande Road. J. Powell says the exposure has deteriorated greatly from its former glory.</p> <p>Sampled 9/20/2023, by A. Sadowski and A. Yokel-Deliduka.</p>
Field sample ID	Ess243r2	
Map unit	Mcge	
TRS location	S17 T17N R18E	
Latitude (degrees)	46.96291	
Longitude (degrees)	-120.60363	
Elevation (ft)	1,865	
Age $\pm 2\sigma$		No older than 9.54 ± 0.49 Ma (MDA, calculated using MLA)



Site Photos (photo number 7833). A. Yokel-Deliduka pointing at sample location (red box). Loose matrix sand collected between cobbles.

LUMINESCENCE DATING

Overview

Luminescence dating estimates the time that has passed since sandy (or silty) sediment was deposited and buried. Following sediment deposition, environmental radiation causes electrons in minerals to jump into metastable, higher-energy electron traps. The technique assumes that this occurs at a predictable rate, such that older sediment contains proportionately more electrons in traps. The technique functions by measuring how much light electrons emit when released from traps. This is done by subjecting the sample to a pulse of activation energy that knocks the electrons out of their metastable traps; their return to a lower energy level emits light. The amount of light emitted is proportional to the time since deposition of the sample—meaning that more light is indicative of an older sample. OSL uses optical light to stimulate luminescence from quartz, whereas IRSL uses infrared light and on potassium feldspar. Exposure to daylight restores electrons from their elevated spin cycles to their more stable, lowest-energy, orbitals and thus resets the signal. Samples for luminescence dating therefore need to be from deposits not exposed to light since their deposition, and the samples need to be collected without exposure to light.

Sample Collection and Preparation

We first removed at least 5 cm of sand from a sand exposure and then pounded a 4.2-cm inner diameter, 30.5-cm-long steel tube (1-5/8-inch electrical conduit) into the in-place sand (preferably surrounded by least 30 cm of undisturbed sand on all sides). We retrieved the tube by digging out the surrounding material until we could remove and seal the tube without loss of sand from inside the tube. We sealed the sample tube with opaque metal foil (heater-duct tape) and rubber caps. We collected some of the removed host material sand into a plastic zip-lock bag for environmental dose rate measurements, and packed sand tightly into a small, well-sealed glass or plastic vial (such as a 35-mm film canister) for field moisture content assessment. The lab analyzed the natural luminescence of mineral separates from sand from the core of the steel tube, which had not been exposed to light since deposition.

Analytical Methods

Our samples were analyzed by Sebastien Huot (Illinois State Geological Survey), whose report (included in the Data Supplement) describes the analytical methods.

Results

We collected and analyzed three samples: one from eolian loess and two from alluvial sand. The loess yielded acceptable results. The alluvial sand sites contained anthropogenic radioisotope cesium-137. See Data Supplement and Table E2 for details.

Table E2. Infrared-stimulated luminescence (IRSL) ages from the Ellensburg South 7.5-minute quadrangle. See Data Supplement for full analytical results.

Site ID	GD08	Luminescence age dates sand deposition 1 m below ground surface ground surface from a hand dug exposure next to a dirt road. This is exposure is from an alluvial fan with a fault escarpment. This age would constrain the age of faulting, especially where compared to the unfaulted surface of site GD09. The field setting is a north-facing hand dug exposure north of a fence line and at the foot of a vegetation anomaly (very green grass trending west-east). We suspect this site was disturbed based on results containing anthropogenic ¹³⁷ Cs. Sampled 9/6/2023, by A. Sadowski and A. Yokel-Deliduka
Field sample ID	Ess225	
Map unit	Qaf2	
TRS location	S23 T17N R18E	
Latitude (degrees)	46.94321	
Longitude (degrees)	-120.54999	
Elevation (ft)	1,490	
Age ±2σ		5.9 ±1.2 ka

**Site Photo (photo number 7513).** Sample collected along fence-lined dirt road on farmland owned by Rob Acheson. Given the presence of anthropogenic ¹³⁷Cs and abundant organic material, we suspect soil development may have affected portions of this exposure near the fenceline.

Site ID	GD09	Luminescence age dates sand deposition ~2 m below the ground surface from a hand dug exposure below a dirt road. This exposure is from an alluvial fan that lacks fault escarpments. This age would have dated alluvial fan deposition and provided a baseline for determining the age of faulting on the faulted alluvial fan surface of age site GD08. The field setting is a northeast-facing, hand-dug exposure above a canal. We suspect this site was disturbed based on results containing anthropogenic ¹³⁷ Cs. Sampled 9/6/2023, by A. Sadowski and A. Yokel-Deliduka.
Field sample ID	Ess224	
Map unit	Qaf2	
TRS location	S23 T17N R18E	
Latitude (degrees)	46.94476	
Longitude (degrees)	-120.55103	
Elevation (ft)	1,481	
Age ±2σ		5.8 ±1.6 ka

**Site Photo (photo number 7490).** Sample collected down from dirt road and above a canal on farmland owned by Rob Acheson. Given the presence of anthropogenic ¹³⁷Cs and abundant organic material sampled we suspect some soil development may have affected portions of this exposure at this roadside slough.

Table E2 continued.

Site ID	GD10	Luminescence age dates loess deposition ~1 m below the top of a loess mound. The field setting is a north-facing hand dug exposure near Durr Road on Manastash Ridge. Sampled 8/29/2023, by A. Sadowski and A. Yokel-Deliduka.
Field sample ID	Ess167	
Map unit	Ql	
TRS location	S34 T17N R18E	
Latitude (degrees)	46.91791	
Longitude (degrees)	-120.56891	
Elevation (ft)	2,558	
	Age $\pm 2\sigma$	3.0 \pm 0.4 ka



Site Photo (photo number 7400). Collected from loess mound on Manastash Ridge. 'Manastash mound' is about 1 m tall.

